AERO

NATIONAL ADVISORY COMMITTEE FOR AERONAUTICS

REPORT No. 746

DRAG AND PROPULSIVE CHARACTERISTICS OF AIR-COOLED ENGINE-NACELLE INSTALLATIONS FOR LARGE AIRPLANES

By ABE SILVERSTEIN and HERBERT A. WILSON, Jr.

1942

AERONAUTIC SYMBOLS

1. FUNDAMENTAL AND DERIVED UNITS

	Symbol	Metric		English	
		Unit	Abbreviation	Unit	Abbreviation
Length	l	meter	m	foot (or mile)	ft (or mi)
Time	t	second	s	second (or hour)	sec (or hr)
Force	F	weight of 1 kilogram	kg	weight of 1 pound	lb
Power	P	horsepower (metric)		horsepower	hp
Speed	V	kilometers per hour	kph	miles per hour	mph
		meters per second	mps	feet per second	fps

2. GENERAL SYMBOLS

W Weight $= mg$

g Standard acceleration of gravity $= 9.80665$ m/s^2 or 32.1740 ft/sec^2

m Mass $= \frac{W}{g}$

I Moment of inertia $= mk^2$. (Indicate axis of radius of gyration k by proper subscript.)

μ Coefficient of viscosity

ν Kinematic viscosity

ρ Density (mass per unit volume)

Standard density of dry air, 0.12497 kg-m^{-4}-s^2 at 15° C and 760 mm; or 0.002378 lb-ft^{-4} sec^2

Specific weight of "standard" air, 1.2255 kg/m^3 or 0.07651 lb/cu ft

3. AERODYNAMIC SYMBOLS

S Area

S_w Area of wing

G Gap

b Span

c Chord

A Aspect ratio, $\frac{b^2}{S}$

V True air speed

q Dynamic pressure, $\frac{1}{2}\rho V^2$

L Lift, absolute coefficient $C_L = \frac{L}{qS}$

D Drag, absolute coefficient $C_D = \frac{D}{qS}$

D_0 Profile drag, absolute coefficient $C_{D0} = \frac{D_0}{qS}$

D_i Induced drag, absolute coefficient $C_{Di} = \frac{D_i}{qS}$

D_p Parasite drag, absolute coefficient $C_{Dp} = \frac{D_p}{qS}$

C Cross-wind force, absolute coefficient $C_C = \frac{C}{qS}$

i_w Angle of setting of wings (relative to thrust line)

i_t Angle of stabilizer setting (relative to thrust line)

Q Resultant moment

Ω Resultant angular velocity

R Reynolds number, $\rho \frac{Vl}{\mu}$ where l is a linear dimension (e.g., for an airfoil of 1.0 ft chord, 100 mph, standard pressure at 15° C, the corresponding Reynolds number is 935,400; or for an airfoil of 1.0 m chord, 100 mps, the corresponding Reynolds number is 6,865,000)

α Angle of attack

ϵ Angle of downwash

α_0 Angle of attack, infinite aspect ratio

α_i Angle of attack, induced

α_a Angle of attack, absolute (measured from zero-lift position)

γ Flight-path angle

REPORT No. 746

DRAG AND PROPULSIVE CHARACTERISTICS OF AIR-COOLED ENGINE-NACELLE INSTALLATIONS FOR LARGE AIRPLANES

By ABE SILVERSTEIN and HERBERT A. WILSON, Jr.

Langley Memorial Aeronautical Laboratory

Langley Field, Va.

NATIONAL ADVISORY COMMITTEE FOR AERONAUTICS

HEADQUARTERS, 1500 NEW HAMPSHIRE AVENUE NW., WASHINGTON, D. C.

Created by act of Congress approved March 3, 1915, for the supervision and direction of the scientific study of the problems of flight (U. S. Code, title 50, sec. 151). Its membership was increased to 15 by act approved March 2, 1929. The members are appointed by the President, and serve as such without compensation.

GEORGE W. LEWIS, *Director of Aeronautical Research* — JOHN F. VICTORY, *Secretary*

HENRY J. E. REID, *Engineer-in-Charge, Langley Memorial Aeronautical Laboratory, Langley Field, Va.*

SMITH J. DEFRANCE, *Engineer-in-Charge, Ames Aeronautical Laboratory, Moffet Field, Calif.*

EDWARD R. SHARP, *Administrative Officer, Aircraft Engine Research Laboratory, Cleveland Airport, Cleveland, Ohio*

TECHNICAL COMMITTEES

AERODYNAMICS
POWER PLANTS FOR AIRCRAFT
AIRCRAFT MATERIALS
AIRCRAFT STRUCTURES
INVENTIONS & DESIGNS
OPERATING PROBLEMS

Coordination of Research Needs of Military and Civil Aviation

Preparation of Research Programs

Allocation of Problems

Prevention of Duplication

Consideration of Inventions

LANGLEY MEMORIAL AERONAUTICAL LABORATORY

LANGLEY FIELD, VA.

AMES AERONAUTICAL LABORATORY

MOFFETT FIELD, CALIF.

AIRCRAFT ENGINE RESEARCH LABORATORY

CLEVELAND AIRPORT, CLEVELAND, OHIO

Conduct, under unified control, for all agencies, of scientific research on the fundamental problems of flight.

OFFICE OF AERONAUTICAL INTELLIGENCE

WASHINGTON, D. C.

Collection, classification, compilation, and dissemination of scientific and technical information on aeronautics

REPORT No. 746

DRAG AND PROPULSIVE CHARACTERISTICS OF AIR-COOLED ENGINE-NACELLE INSTALLATIONS FOR LARGE AIRPLANES

By Abe Silverstein and Herbert A. Wilson, Jr.

SUMMARY

An investigation is in progress in the NACA full-scale wind tunnel to determine the drag and the propulsive efficiency of nacelle-propeller arrangements for a large range of nacelle sizes. In contrast with the usual tests with a single nacelle, these tests were conducted with nacelle-propeller installations on a large model of a four-engine airplane. Data are presented on the first part of the investigation, covering seven nacelle arrangements with nacelle diameters from 0.53 to 1.5 times the wing thickness. These ratios are similar to those occurring on airplanes weighing from about 20 to 100 tons.

The results show the drag, the propulsive efficiency, and the over-all efficiency of the various nacelle arrangements as functions of the nacelle size, the propeller position, and the airplane lift coefficient. The effect of the nacelles on the aerodynamic characteristics of the model is shown for both propeller-removed and propeller-operating conditions.

INTRODUCTION

The trend toward increasing airplane size unaccompanied by a corresponding increase in the diameter of air-cooled engines has led to designs in which the engine-nacelle diameter is equal to, or even less than, the wing thickness. In contrast, the engine-nacelle diameter for small high-performance airplanes is from four to five times the wing thickness. Data on nacelle installations are available chiefly in the range of the ratio of nacelle diameter to wing thickness from 1.5 to 2.0. In order to investigate more completely the entire range, tests are being conducted in the NACA full-scale wind tunnel for ratios of nacelle diameter to wing thickness varying from 0.53 to 4.0. This paper presents the results obtained for the smaller nacelles with diameters varying from 0.53 to 1.5 times the wing thickness.

In contrast with the usual tests of a single nacelle, this investigation has been made with four nacelles on a midwing monoplane model simulating a modern four-engine airplane. By this method not only was the drag measured with greater certainty, but the effects of the nacelles and the propeller slipstream on the airplane characteristics were also determined. Nacelles of three diameters were tested, each for several positions of the propeller ahead of the wing leading edge. The four-engine model with the nacelles of different size may be considered to represent airplanes of different size; the model with the largest nacelle may simulate a 20-ton airplane, and the model with the smallest nacelle may simulate one of 100 tons.

SYMBOLS

α	angle of attack of fuselage reference axis relative to wind axis, degrees
q	free-stream dynamic pressure, pounds per square foot
S	wing area, square feet
$\bar{c}$	mean chord of wing (area/span), feet
t_w	maximum wing thickness (average for two lateral nacelle locations), feet
D_P	propeller diameter, feet
D_N	maximum nacelle diameter, feet
F	maximum cross-sectional area of nacelle, square feet
V	airspeed, feet per second
L	lift, pounds
D	drag, pounds
D_c	power-off drag of model with engine-nacelle installation, pounds
M	pitching moment, foot-pounds
C_L	lift coefficient (L/qS)
C_D	drag coefficient (D/qS) (Subscript w refers to power-off drag of model with *bare wing;* subscript c, to power-off drag of model with *engine-nacelle installation.*)
$\Delta C_D = C_{D_c} - C_{D_w}$	
C_{D_F}	drag coefficient for single nacelle based on maximum cross-sectional area ($\Delta C_D S/4F$)
C_m	pitching-moment coefficient ($M/q\bar{c}S$)
R	resultant force of propeller-nacelle-wing combination, pounds
T	thrust of propellers operating in front of body (tension in propeller shafts), pounds
ΔD	increase in drag of body due to action of propellers, pounds
$T-\Delta D$	effective thrust of propeller-nacelle installation
T_0	index thrust

P power input to all propellers

η propulsive efficiency $\left[\frac{(T-\Delta D)V}{P}\right]$

η_t over-all efficiency $\left[\eta(C_{D_w}/C_{D_c})\right]$

T_{c_0}' index thrust coefficient $\left(\frac{P\eta_0}{qSV}\right)$

η_0 index efficiency (η at $C_L=0.25$)

n propeller speed, revolutions per second

β propeller blade angle at 0.75 radius, degrees

δ_f flap deflection from closed position, degrees

MODEL AND TEST EQUIPMENT

The tests were conducted in the NACA full-scale wind tunnel, which is described in reference 1. The model is a metal-covered midwing monoplane with a span of 37.25 feet. The symmetrical wing sections are tapered in thickness from the NACA 0018 at the root to the NACA 0010 at the tip. The wing plan form tapers 4:1 from a root chord of 7.28 feet, and the wing area is 172 square feet. Split trailing-edge flaps with an average chord of 0.15c extend over the middle 60 percent of the span with the exception of a short gap at the fuselage. The angle of wing setting to the fuselage reference line is 4.6°. The principal dimensions of the model and the nacelle for each of the test arrangements are shown in figure 1. Figures 2 to 5 show the model installed in the full-scale tunnel.

A summary of the nacelle installations investigated is shown in table I.

TABLE I

Test	Nacelle diameter (in.)	$\frac{D_N}{t_w}$ (1)	Propeller diameter (in.)	Propeller location (2)	Figure showing details
1	Bare-wing model, no cowling				2
2a	20	1.50	39	0.40c	1 (c)
2b	20	1.50	39	.25c	5
3a	10.4	.78	39	.40c	4
3b	10.4	.78	39	.25c	1 (b)
4a	7	.53	24	.40c	1 (a)
4b	7	.53	24	.25c	1 (a)
4c	7	.53	24	.13c	3

[1] Thickness t_w is the average of wing thicknesses at the nacelle locations.
[2] Chord c is the local chord at each propeller location.

Four three-blade metal propellers of 39-inch diameter were used for the tests with the nacelles 20 and 10.4 inches in diameter. Blade dimensions and sections for the propeller are given in figure 6. Four two-blade metal propellers of 24-inch diameter and Bureau of Aeronautics Drawing No. 4412 were used for the tests with the 7-inch nacelles. The propellers were driven through extension shafts by 25-horsepower alternating-current motors enclosed within the wing. The speed of the propellers was regulated by varying the frequency of the motor-current supply and was measured with an electric tachometer. The propeller torques were determined from an electric calibration of the motors.

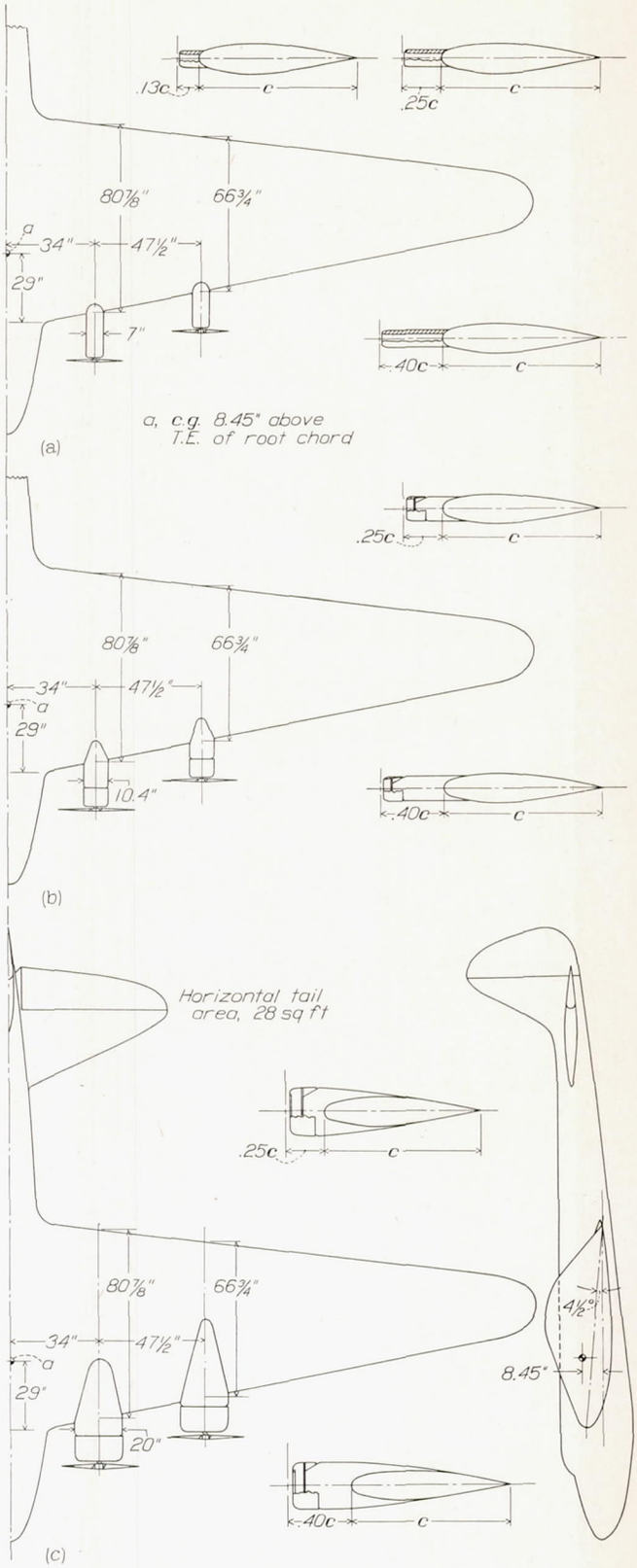

(a) The 7-inch nacelles; $D_N/t_w=0.53$.
(b) The 10.4-inch nacelles; $D_N/t_w=0.78$.
(c) The 20-inch nacelles; $D_N/t_w=1.5$.

FIGURE 1.—Diagram of model showing arrangements of the nacelles.

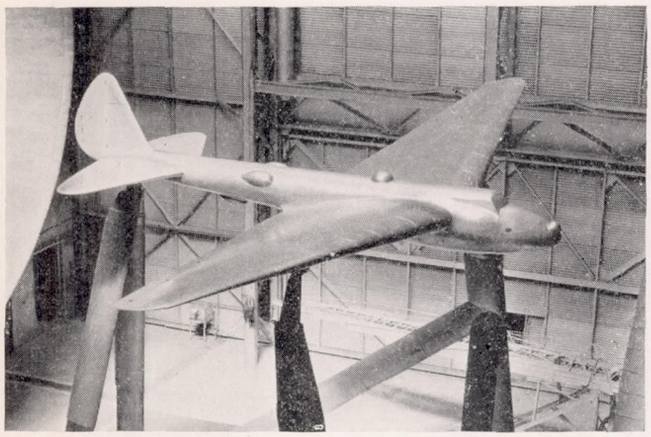

FIGURE 2.—Installation of model without nacelles in the NACA full-scale wind tunnel.

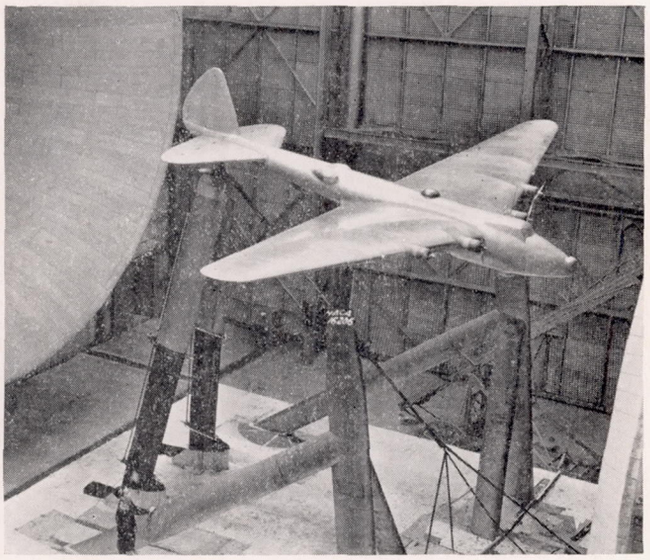

FIGURE 3.—Installation of model with 7-inch nacelles and 0.13c propeller location in the NACA full-scale wind tunnel.

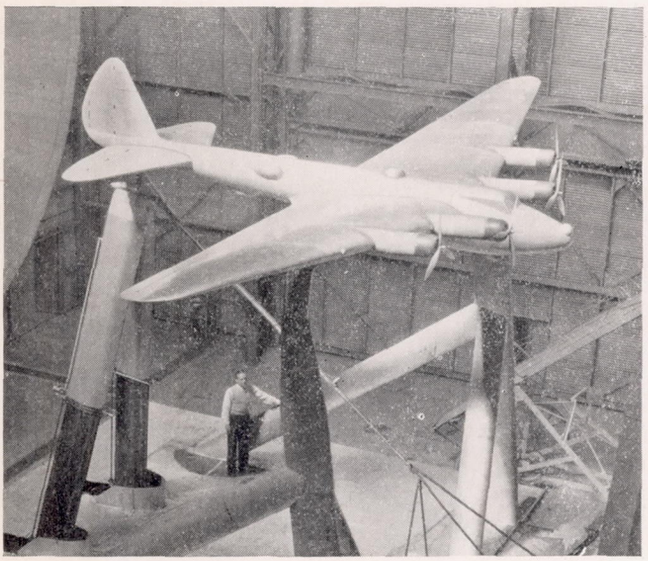

FIGURE 4.—Installation of model with 10.4-inch nacelles and 0.40c propeller location in the NACA full-scale wind tunnel.

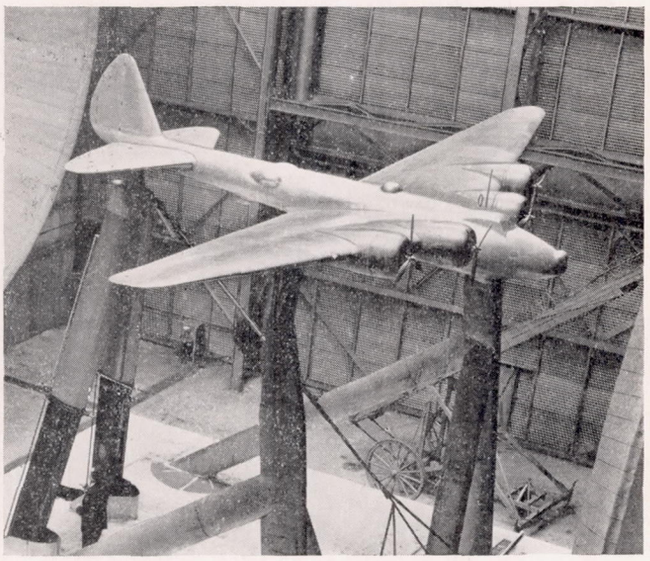

FIGURE 5.—Installation of model with 20-inch nacelles and 0.25c propeller location in the NACA full-scale wind tunnel.

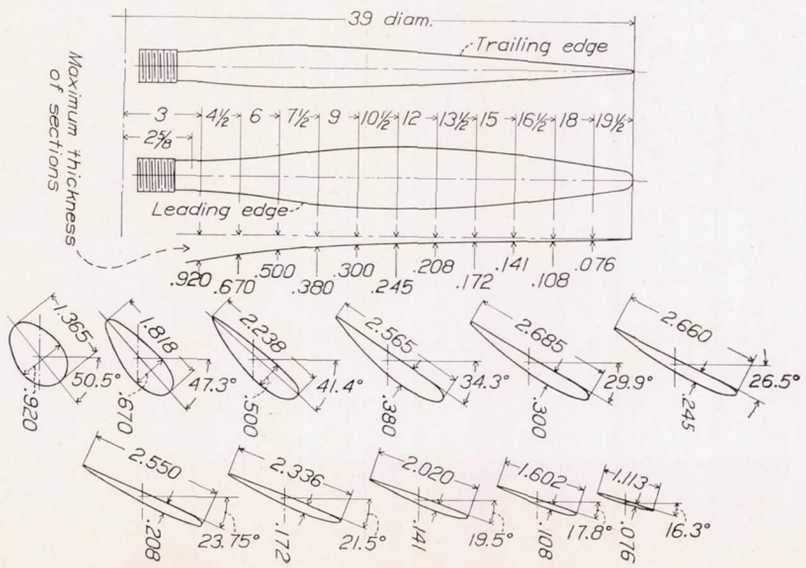

FIGURE 6.—Blade dimensions for three-blade model propellers. All linear dimensions given in inches.

Figure 7 is a diagram of a representative cowling-nacelle installation, with the dimensions for the cowling given as fractions of the cowling diameter. The cowling was geometrically similar to the one designated cowling C in reference 2. Perforated metal plates were used to furnish a resistance similar to that of a well-baffled engine. The number of holes in the plates was adjusted to give a value of conductivity K (reference 3) of approximately 0.10. The exit slot of the cowling was proportioned to provide a pressure drop across the engine of $0.35q$, corresponding to sufficient cooling for flight at 200 miles per hour. It is assumed that cowling flaps or other adjustments will be provided for different flight conditions. Smooth fairing of the nacelles into

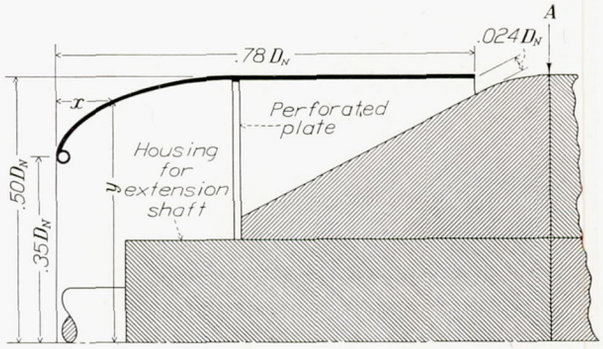

FIGURE 7.—Dimensions of cowling and cowling arrangement.

Cowling profile

x/D_N	y/D_N	x/D_N	y/D_N
0	0.350	0.115	0.460
.005	.378	.135	.467
.010	.387	.154	.474
.019	.399	.192	485
.038	.416	.231	.493
.058	.431	.269	.498
.077	.441	.308	.500
.096	.452	.335	.500

the wing was provided by small fillets at the junctures of the wing and the nacelles (figs. 3, 4, and 5). In order to change the propeller position from $0.25c$ to $0.40c$, the nacelle was extended by inserting a cylindrical section at A (fig. 7). For the tests with no cooling air, the perforations in the metal plates were sealed. The 7-inch nacelles were not provided with perforated plates and cooling-air passages because a preliminary analysis indicated the effects of the cooling-air flow to be immeasurable.

TESTS

With the propellers removed from the model, measurements of aerodynamic forces and pitching moment were made at an airspeed of about 60 miles per hour for all the nacelle installations over an angle-of-attack range from zero lift through the stall. Scale effect on the drag at low lift coefficients was also measured over a range of airspeeds from 30 to 100 miles per hour.

With the propellers operating, propulsive characteristics of the nacelle-propeller installations were determined for the attitude in which the thrust axes were parallel to the relative wind and for lift coefficients approximating those for high-speed and climbing flight. In addition to the usual aerodynamic forces and pitching moment, the power-on measurements included the power input to the propellers and the propeller speed. In the propeller tests the torque was held constant and the tunnel airspeed was increased in steps from 30 to 100 miles per hour; the propeller speed was then reduced until zero thrust was reached. The effect of the propeller operation upon the lift and the pitching moment was determined at a tunnel speed of approximately 60 miles per hour for several thrust conditions and with the propellers freewheeling.

The conductivity of the perforated cowling plate and the air flow through the cowling were determined from measurements of the pressure drop across the plate and of the dynamic and the static pressures at the cowling exit.

PROPELLER-REMOVED CHARACTERISTICS

The aerodynamic characteristics of the four-engine model with the propellers removed are shown in figures 8 to 15 for the various arrangements tested. These data were obtained at a tunnel airspeed of about 60 miles per hour, which corresponds to a Reynolds number of 2,500,000 based on the average wing chord of 4.62 feet. The coefficients are based on a wing area of 172 square feet and are corrected for wind-tunnel effects. Pitching-moment coefficients are computed about a center of gravity located as shown in figure 1. The tests were made with cooling air flowing through the cowling corresponding to that required for high-speed flight.

Drag.—Scale effects on the airplane drag coefficients for the nacelle arrangements tested are shown in figure 16 at the assumed high-speed lift coefficient of 0.25. Reference curves showing the scale effects on the model without nacelles are given in figure 17 for values of C_L from −0.2 to 0.7.

At low lift coefficients, the curves of figures 16 and 17 show the negative-slope characteristic of plots of skin-friction drag coefficient against Reynolds number. At high lift coefficients, where the skin friction is only a small part of the total drag, the drag coefficient is about the same over the range of airspeeds tested. This result, which is also representative of the various cowling installations, is shown in figure 17 for the bare-wing model. Particularly interesting is the fact that the increment of drag due to the nacelle installations is essentially independent of the test speed.

The increments of the airplane drag coefficient ΔC_D due to the presence of four nacelles are plotted against the ratio of the nacelle diameter to the wing thickness in figure 18. These increments are given for several lift coefficients, both with air flowing through the cowling (fig. 18 (a)) and with the cowling closed (fig. 18 (b)). The values were taken from the scale-effect curves (fig. 16) at a test speed of 100 miles per hour.

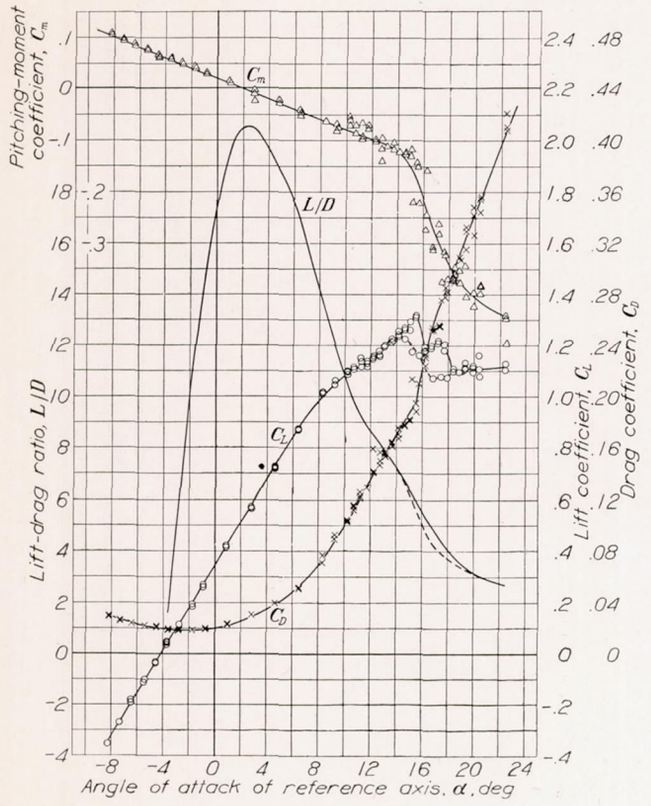

FIGURE 8.—Aerodynamic characteristics of model without nacelles.

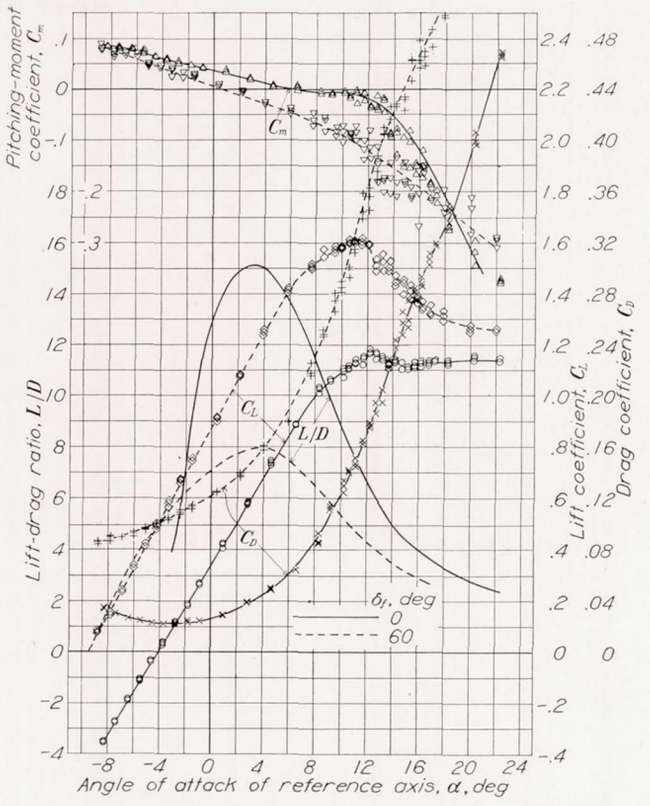

FIGURE 9.—Aerodynamic characteristics of model with 20-inch nacelles and 0.40c propeller location.

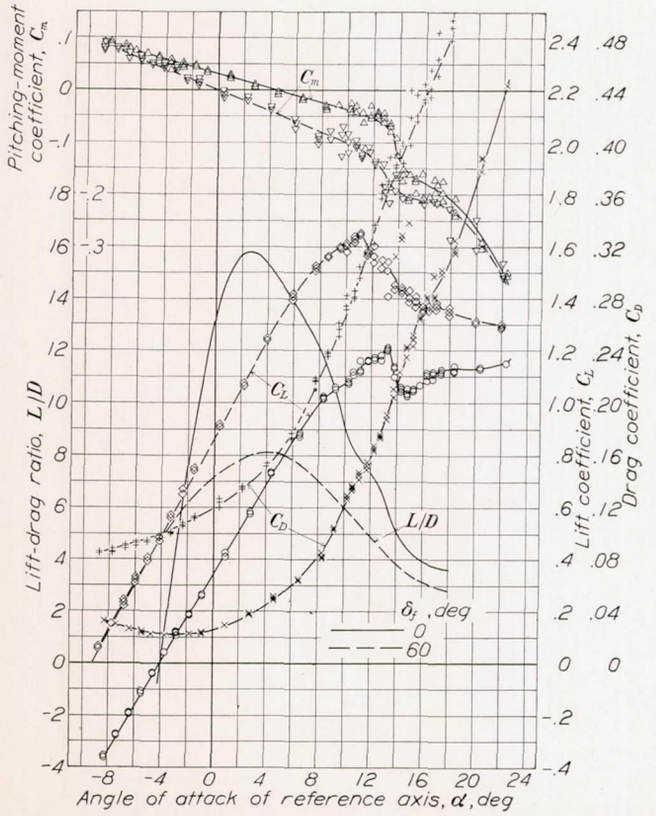

FIGURE 10.—Aerodynamic characteristics of model with 20-inch nacelles and 0.25c propeller location.

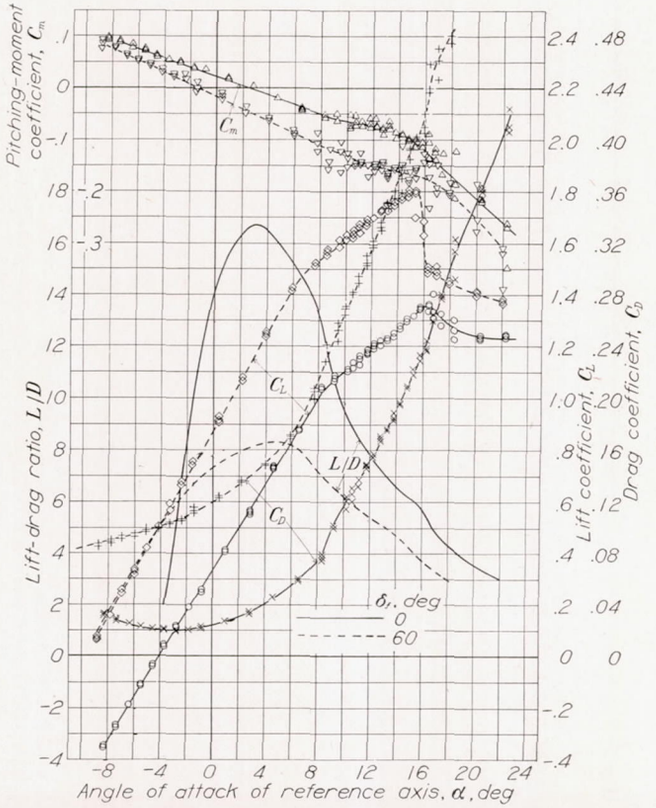

FIGURE 11.—Aerodynamic characteristics of model with 10.4-inch nacelles and 0.40c propeller location.

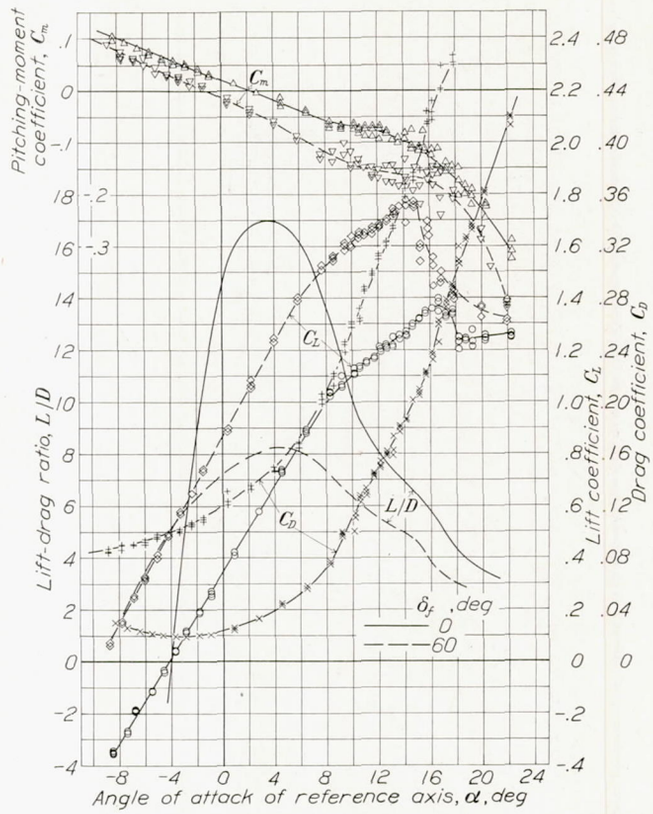

FIGURE 12.—Aerodynamic characteristics of model with 10.4-inch nacelles and 0.25c propeller location.

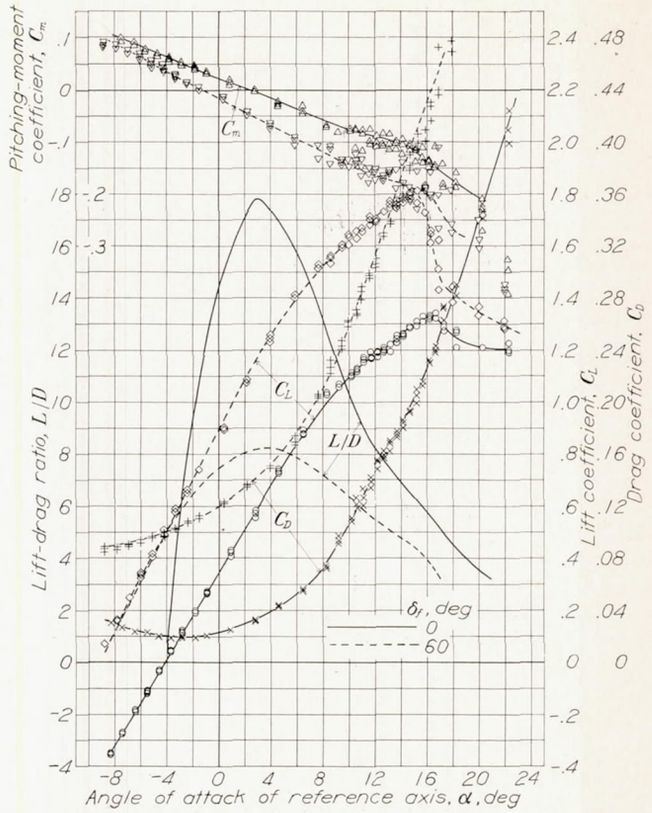

FIGURE 13.—Aerodynamic characteristics of model with 7-inch nacelles and 0.40c propeller location.

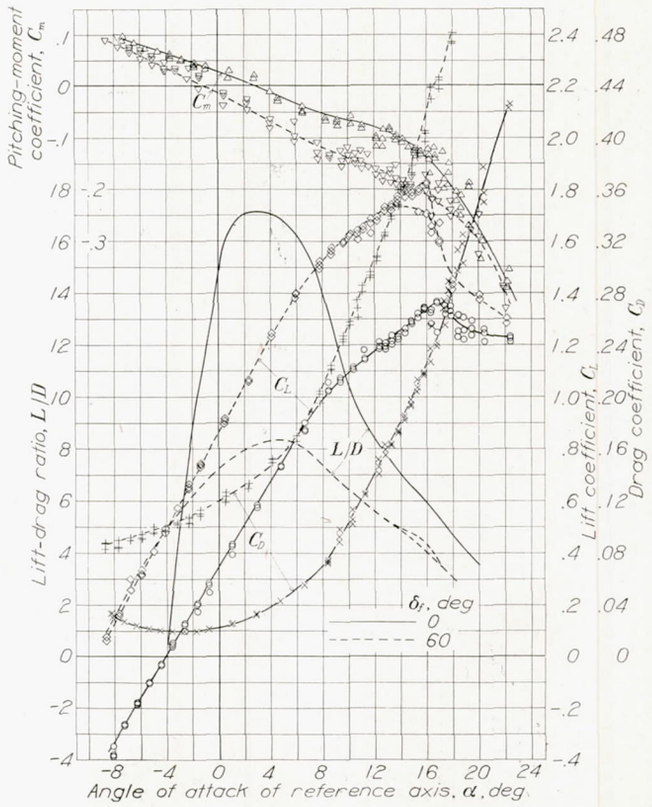

FIGURE 14.—Aerodynamic characteristics of model with 7-inch nacelles and 0.25c propeller location.

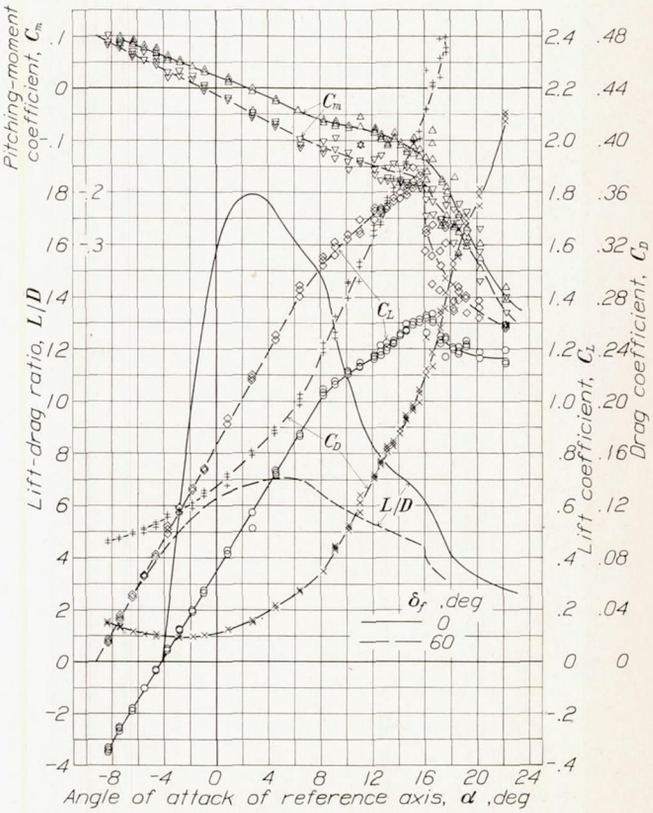

FIGURE 15.—Aerodynamic characteristics of model with 7-inch nacelles and 0.13c propeller location.

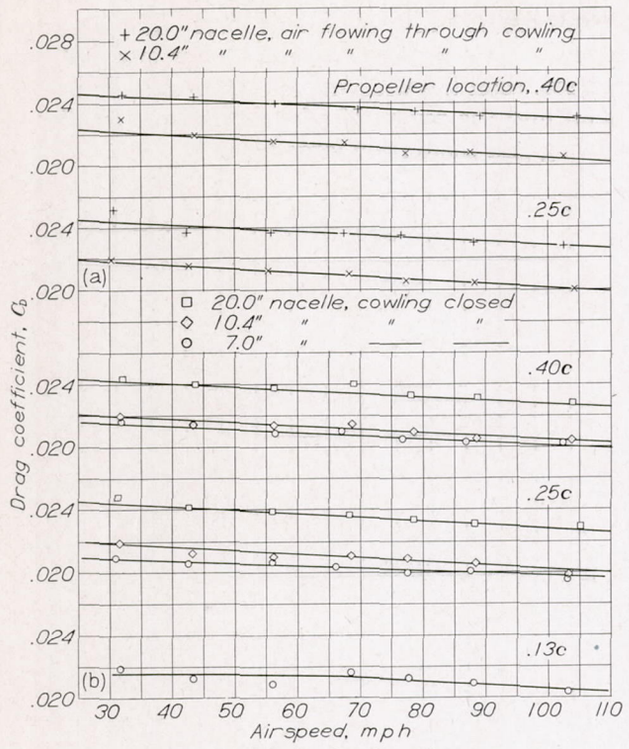

(a) Air flowing through cowling.
(b) Cowling closed.

FIGURE 16.—Scale effect on drag coefficient at C_L=0.25.

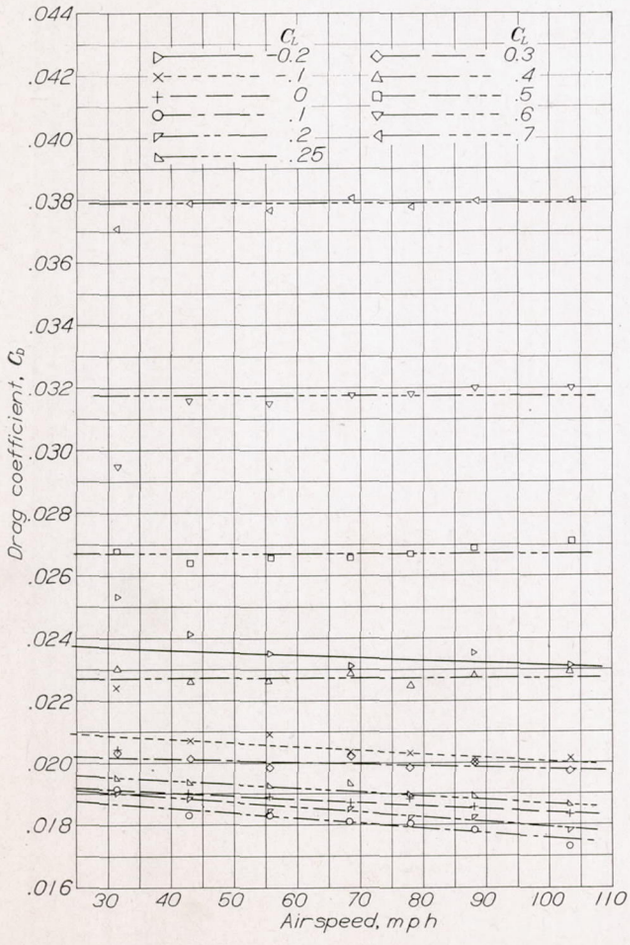

FIGURE 17.—Scale effect on the model without nacelles for the range of lift coefficients.

If the nacelle drag increments for the cases of no air flow and with an air flow sufficient for cooling in high-speed flight are compared, it is seen that the effect of the air flow on the drag coefficient is slight. This result has been noted in previous investigations in which the cooling-air flow was properly regulated (reference 4). At high lift coefficients the drag was reduced in some cases by the air flowing through the cowling.

In order to demonstrate the magnitude of the nacelle drag for airplanes of different size, it will be assumed that the drag coefficient of an efficient airplane without nacelles is 0.0150 at a high-speed lift coefficient of 0.15. For a 75-ton airplane in which the ratios of D_N/t_w may be about 0.6, the increment of drag coefficient due to four nacelles with propellers at the 0.25c location (fig. 18 (a)) is 0.0005. Further, if a six-engine installation for an airplane of this size is assumed, the drag coefficient of the nacelles is 0.00075, or 5 percent of the total airplane drag.

For another typical design of a 20-ton four-engine airplane, the ratio of D_N/t_w may be 1.5 with the result that ΔC_D=0.0036 at C_L=0.15. In this case, the drag of the nacelles is 24 percent of the total airplane drag. The relatively great adverse effect of the large nacelles on the small airplane is clearly demonstrated.

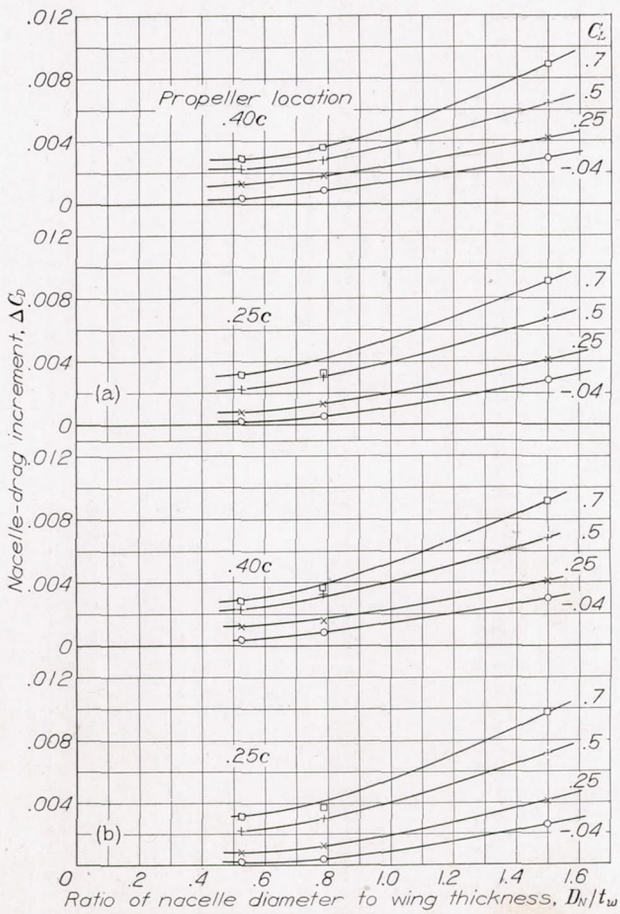

(a) Air flowing through cowling.
(b) Cowling closed.

FIGURE 18.—Drag increments due to nacelles for nacelles of various size and for several lift coefficients.

The drag increments ΔC_D of figure 18 are presented in figure 19 in the form C_{D_F}, which is the drag coefficient for a single nacelle based on the maximum cross-sectional area of the nacelle. The curves of figure 19 are of particular interest in pointing out the relatively large nacelle drag coefficients of the small nacelles at high lift coefficients and the low drag of the short nacelles at low lift coefficients.

It is believed that the prediction of nacelle drag over the range of nacelle sizes tested can be made with considerable accuracy by reference to figure 19.

Lift.—The addition of nacelles to the airplane tends to increase slightly the slope of the lift curve and the increase is about proportional to the nacelle size (figs. 8 to 15). The lift-curve slope was increased about 2½ percent by the four 20-inch nacelles. The high lift is attributed to the increased area added by the nacelles and is consistent with results of previous investigations. The angle of zero lift was also slightly changed by the nacelles; the difference was about 0.2° for the 20-inch nacelles.

The maximum lift coefficient of the airplane with cooling air flowing through the cowling varied with the nacelle installation, as shown in table II.

TABLE II

VALUES OF MAXIMUM LIFT COEFFICIENT

$\frac{D_N}{t_w}$	Propeller location	Maximum lift coefficient	
		$\delta_f=0°$	$\delta_f=60°$
Without nacelles		1.31	
0.53	0.13c	1.33	1.83
.53	.25c	1.35	1.83
.53	.40c	1.32	1.81
.78	.25c	1.37	1.77
.78	.40c	1.36	1.80
1.50	.25c	1.21	1.65
1.50	.40c	1.17	1.60

In a comparison of the maximum lift coefficients, the model with the small nacelles has slightly higher values and the model with the large nacelles has considerably lower values than the model without nacelles. The large decreases in maximum lift coefficient for the installations with nacelle diameters larger than the wing thickness are attributed to different pressure distributions over the upper surface of the nacelle and the adjacent wing surface. Tuft observations (fig. 20) on the upper surface of the airfoil near the rear of the large nacelles at high lift coefficients show the flow spreading out laterally on both sides of the nacelle. This result indicates a higher pressure on the nacelle than on the adjacent wing surface owing to the expansion of the air behind the maximum nacelle section.

The lateral motion of the air in the region of adverse pressure gradient on the wing has a strong destabilizing effect and causes breakdown of the flow. In the case of the cowling with $D_N/t_w=1.5$, the maximum lift coefficient was decreased about 9 percent. For an unpublished case of a cowling installation with $D_N/t_w=3.7$, the maximum lift coefficient was decreased 16.5 percent. In case the nacelle diameter is about equal to or less than the wing thickness, the nacelle does not extend into the region of adverse pressure gradient on the wing and there is no large taper to the nacelle with

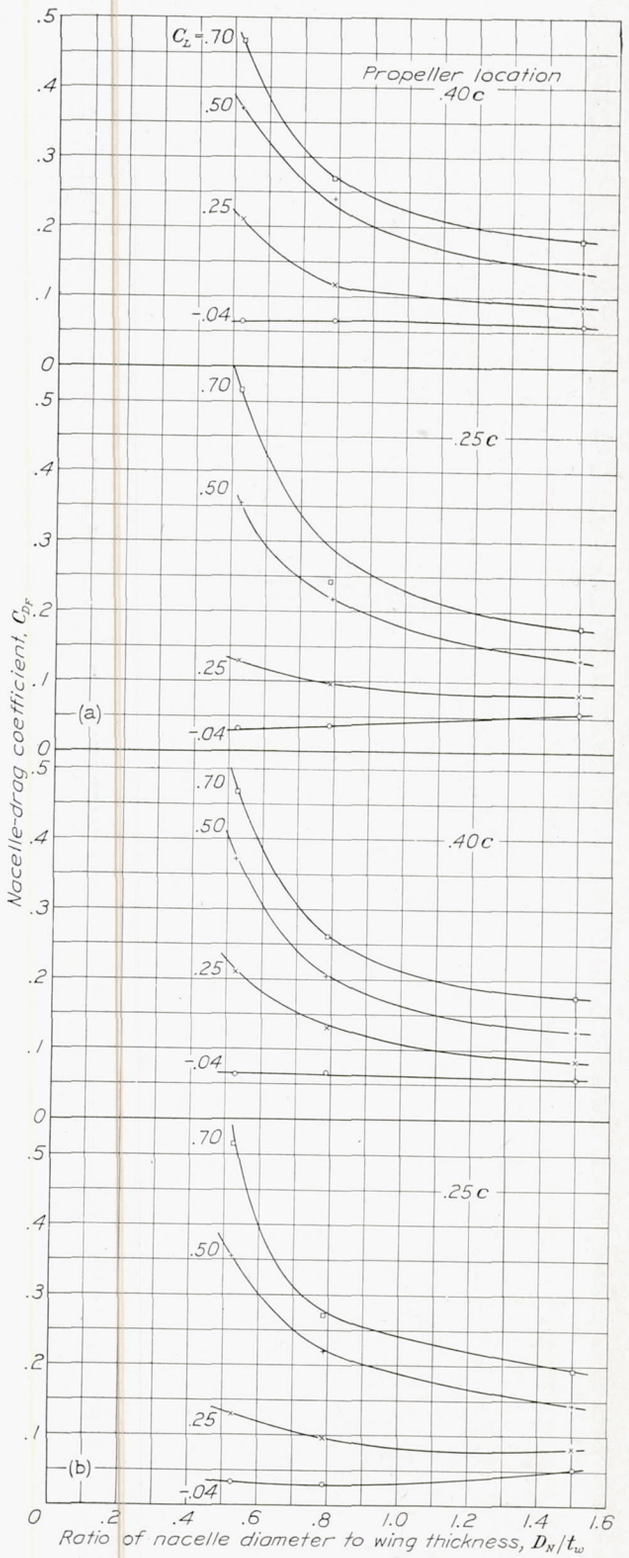

(a) Air flowing through cowling.
(b) Cowling closed.

FIGURE 19.—Nacelle drag coefficient for nacelles of various size and for several lift coefficients.

the attendant adverse pressure gradient. The slight increase in maximum lift coefficient shown by the small nacelles is attributed to the increased surface area of the wing-nacelle combination.

Lift-drag ratio.—Inasmuch as the range of an airplane is about proportional to the value of the maximum lift-drag ratio, the large reductions in the value of maximum lift-drag ratio caused by even the smallest nacelles should be pointed out. In comparison with the assumed case of an airplane without nacelles, the smallest nacelle installation ($D_N/t_w=0.53$) reduced the value of maximum lift-drag ratio by about 14 percent (fig. 21); whereas the large nacelles reduced it by about 25 percent. The results of figure 21 substantiate those of figure 19 in showing that the small nacelles contribute

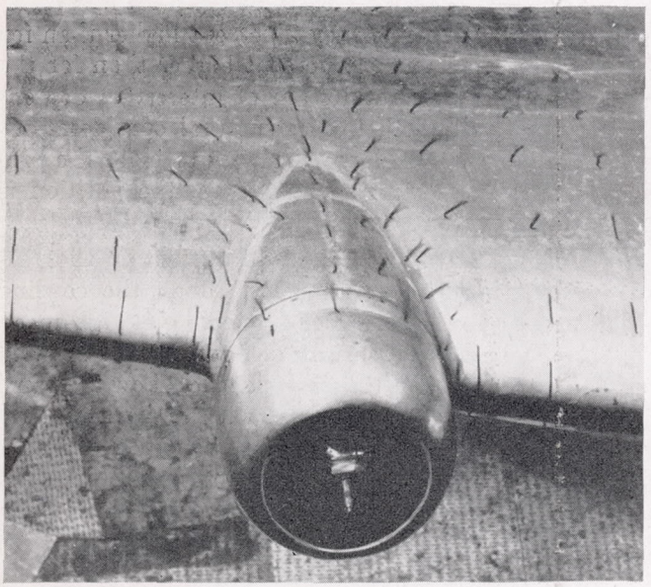

FIGURE 20.—Air flow over upper surface of wing and nacelle. The 20-inch nacelle; 0.25c propeller location; α, 12°.

considerably more drag at the high than at the low lift coefficients. The lift coefficient for the maximum lift-drag ratio for the model is about 0.55.

Pitching moment.—The large nacelles have a marked destabilizing effect on the airplane. This result is shown in figure 22 in which the slopes of curves of the pitching-moment coefficient are plotted against nacelle size. The slopes shown in figure 22 were taken over the straight portions of the pitching-moment curves between $\alpha=-5°$ and 5°. The decreased stability is indicated by the low values of the negative slope. The slope of the pitching-moment curve is decreased by the nacelles even more markedly at high than at low angles of attack, as shown by the slopes in figures 8 and 9 between $\alpha=8°$ and 12°. The decrease of the slope of the pitching-moment curve is attributed to a forward movement of the aerodynamic center of the wing due to the addition of the nacelle surface ahead of the leading edge.

This reasoning is substantiated by figure 22 in which it may be noted that the longer nacelles show greater destabilizing effects. At the high angles of attack, the resultant force on the cowling contributes a large positive moment. Unless this effect is taken into consideration in the tail-plane design, it may lead to instability.

PROPULSIVE AND OVER-ALL EFFICIENCIES

The nacelle drag coefficients alone are an insufficient basis for comparison of the various nacelle-propeller

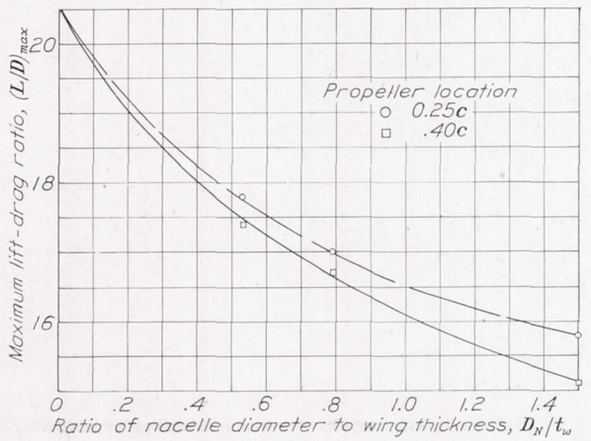

FIGURE 21.—Variation of the maximum lift-drag ratio of the model for nacelles of various size.

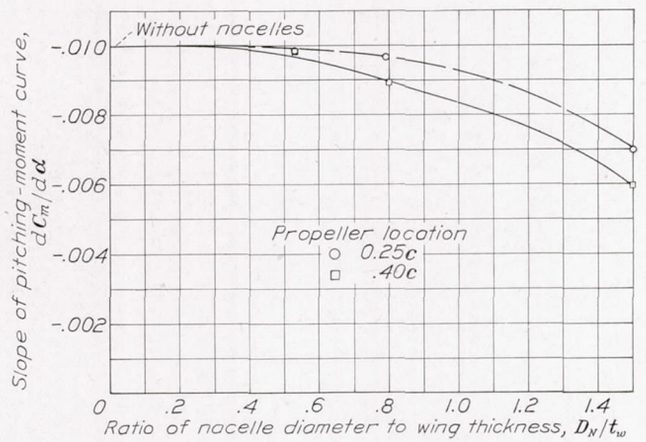

FIGURE 22.—Variation of the slope of the pitching-moment curve of the model for nacelles of various size.

installations. The installations are more properly compared by an over-all efficiency that includes the nacelle-drag increment measured with the propellers removed as well as by the propulsive efficiency. This over-all efficiency η_t is defined as the ratio of the towline power required for the bare-wing model (without nacelles) at a given level-flight speed to the actual power input required at this speed by the model with the nacelle-propeller installations. In this method the over-all efficiency of the bare-wing model is 100 percent and, for a nacelle-propeller installation, is given by

$$\eta_t=\eta(C_{D_w}/C_{D_c})$$

The propulsive efficiency η is the ratio of the effective thrust power to the power input and may be calculated from the relation

$$\eta=\frac{(T-\Delta D)V}{P}$$

The value of the effective thrust $T-\Delta D$ may be computed from the wind-tunnel data by means of the relation

$$T-\Delta D=D_c+R$$

in which D_c and R are the observed readings on the drag scale for propeller-removed and propeller-operating conditions, respectively.

For tests without a lifting surface behind the propeller, $T-\Delta D$ may be calculated from measurements of D_c and R obtained at the same angle of attack and dynamic pressure. When the flow over a lifting surface is influenced by the propeller, the changes in lift as well as in drag should be credited to or charged against the propeller. The change in lift has been allowed for in these results by making measurements of D_c and R at the same lift coefficient instead of at the same angle of attack.

PROPULSIVE EFFICIENCIES

Data have been obtained to show the effect on the propulsive efficiency of variations in the following:

1. Propeller blade angle
2. Nacelle diameter
3. Propeller location
4. Air flowing through cowling
5. Lift coefficient

Propeller blade angle.—The results obtained with the 39-inch-diameter three-blade propellers (figs. 23 to 26) are consistent in indicating that the maximum propulsive efficiency occurs at a blade angle β of about 30°. The envelopes of the efficiency curves are flat, however, and variation in β of $\pm 8°$ from the optimum causes only slight reductions in maximum propulsive efficiency. The two-blade propeller used with the small nacelles also shows maximum propulsive efficiency at $\beta=30°$ (figs. 27 to 29). The envelopes are not flat, and slight variations from the optimum blade angle lead to substantial decreases in maximum propulsive efficiency.

From analysis of figures 23 to 29, it may be concluded that the blade angle for maximum propulsive efficiency is not greatly affected by the location of the propeller with reference to the wing or by the diameter of the nacelle behind the propeller.

Nacelle diameter.—The effect of variation in the nacelle diameter on the maximum propulsive efficiency is shown by a comparison of figures 23 and 24 with figures 25 and 26. For each propeller location, the smaller of the two nacelles shows a slightly lower propulsive efficiency than the larger one. This difference, however, does not exceed 1 percent, which is about the limit of the experimental accuracy. The results of these tests indicate, in the usual range, that the propulsive efficiency is almost independent of the ratio of the propeller to the cowling diameter. It should be noted that the value of zero propulsive efficiency—that is, zero effective thrust—occurs at higher values of V/nD for the large nacelle than for the small one.

Propeller location.—The variation of the propulsive efficiency with propeller location for the three-blade propeller installations is shown by a comparison of figures 23 and 25 with figures 24 and 26. The propeller on the 20-inch nacelles ($D_N/t_w=1.5$) shows about the same maximum propulsive efficiency with the propeller located in either the 0.40c or the 0.25c position. The installation with the 10.4-inch nacelles ($D_N/t_w=0.78$) shows a slightly higher maximum propulsive efficiency with the propeller in the 0.25c position than in the 0.40c position, but the differences are only slightly greater than the limits of experimental accuracy.

The two-blade propeller on the 7-inch-diameter nacelle installation was tested 0.40c, 0.25c, and 0.13c ahead of the wing leading edge. The results (figs. 27 to 29) show the 0.25c location to be the most favorable, with the propulsive efficiency 2 percent higher than for the 0.40c location and 3.5 percent higher than for the 0.13c location. The results are of interest in demonstrating that, although from structural considerations it may be desirable on large airplanes to place the propeller close to the wing leading edge, the position is aerodynamically undesirable.

Air flowing through cowling.—The effect on the propulsive efficiency of air flowing through the cowling corresponding to that required for cooling at high-speed flight is shown by comparison of figures 23 to 26 with figures 30 to 33. The 10.4-inch nacelles show the same maximum propulsive efficiencies with and without air flowing through the cowling. The large nacelles rather consistently show maximum propulsive efficiencies about 1 percent higher for the closed cowlings than for the open ones.

These results indicate that the propulsive efficiencies measured on nacelle installations with no air flowing through the cowling are sufficiently accurate for predicting the values that will be obtained with correct cooling flow. Other nacelle tests with excessive cooling air and poorly designed cowling outlets do not substantiate this conclusion.

Lift coefficient.—The variations in the propulsive efficiencies with airplane lift coefficient are shown in figures 34 to 37. The results are shown for $\beta=23\frac{1}{2}°$, which was chosen as an average flight propeller blade-angle setting for the range of lift coefficients tested. In each case, the maximum propulsive efficiency was obtained at $C_L=0.70$ and the lowest at $C_L=0.25$, with an average difference between them of about 4 percent. The high efficiency at $C_L=0.70$ is due to the favorable effect of the propeller slipstream in decreasing the interference between the nacelle and the wing. The presence of this interference and its effect in increasing the value of C_{D_F} at the higher lift coefficient has previously been noted.

The propulsive efficiency for $C_L=-0.04$, in which case the nacelle axis was parallel to the relative wind, was higher than for the high-speed flight condition.

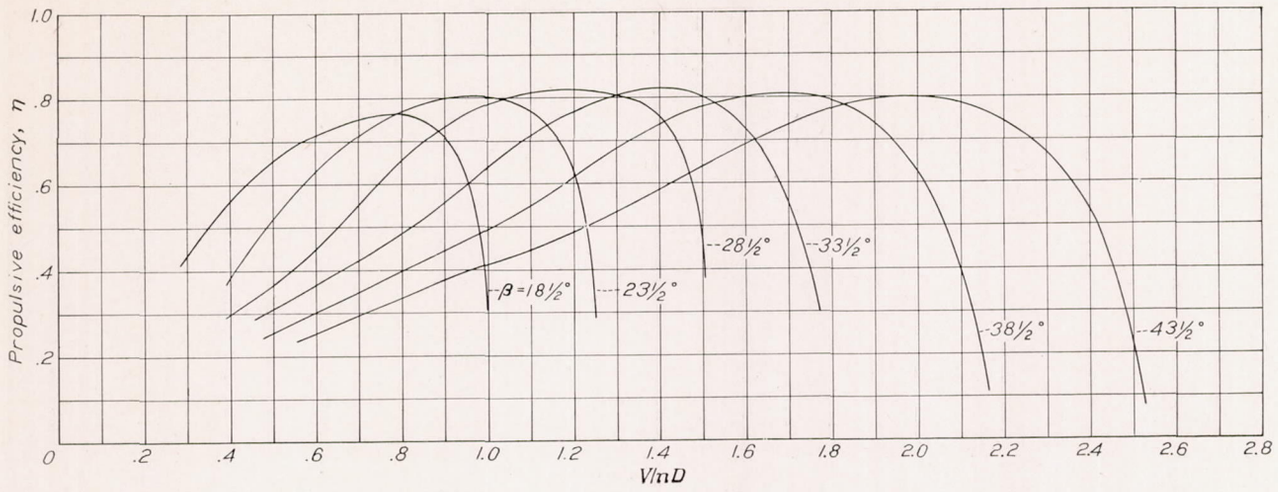

FIGURE 23.—Variation of propulsive efficiency with blade angle. The 20-inch nacelles; 0.40c propeller location; C_L, 0.25; air flowing through cowling.

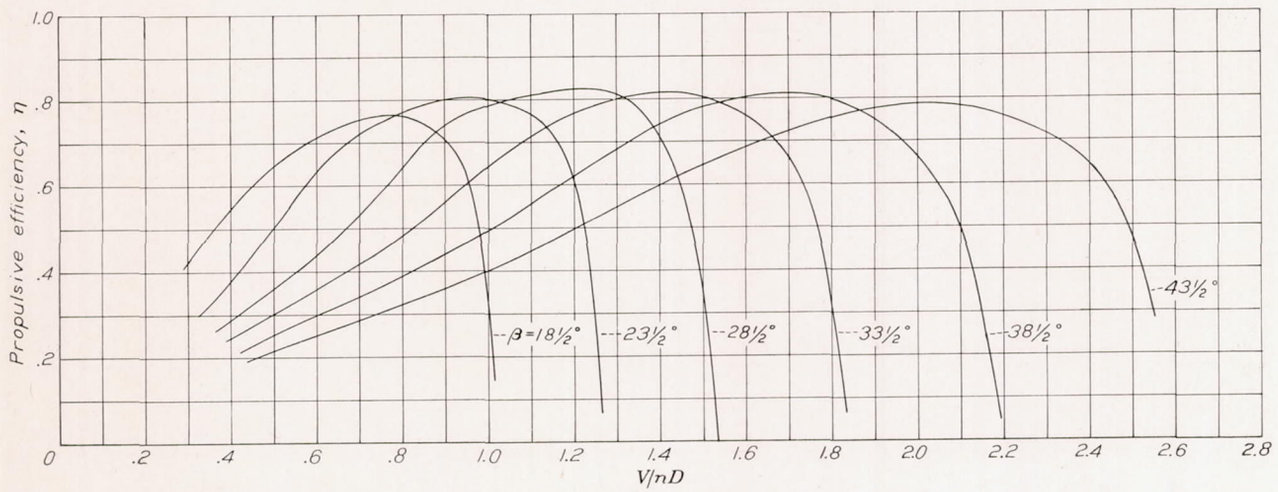

FIGURE 24.—Variation of propulsive efficiency with blade angle. The 20-inch nacelles; 0.25c propeller location; C_L, 0.25; air flowing through cowling.

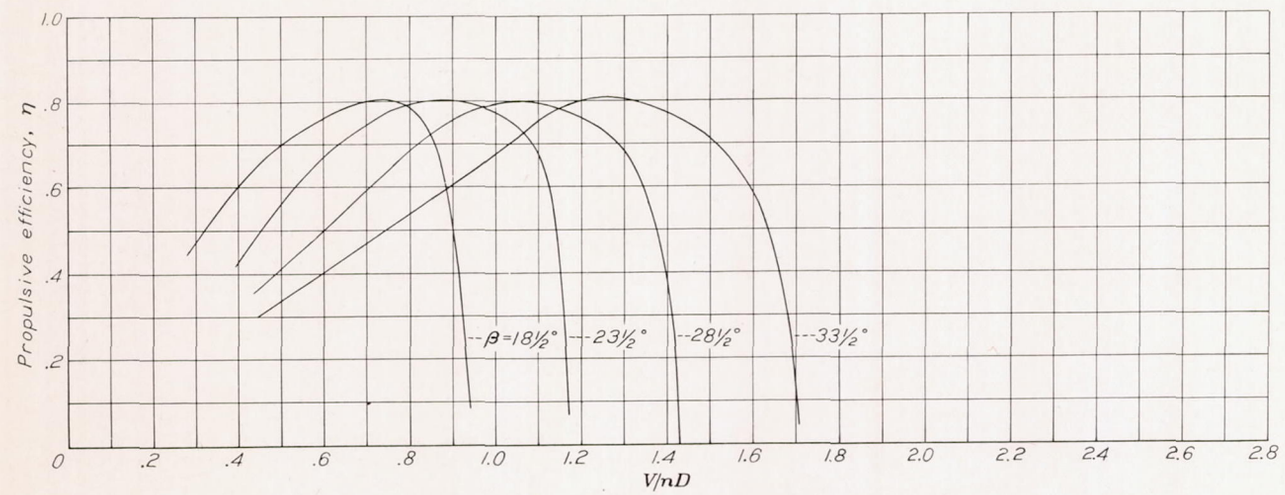

FIGURE 25.—Variation of propulsive efficiency with blade angle. The 10.4-inch nacelles; 0.40c propeller location; C_L, 0.25; air flowing through cowling.

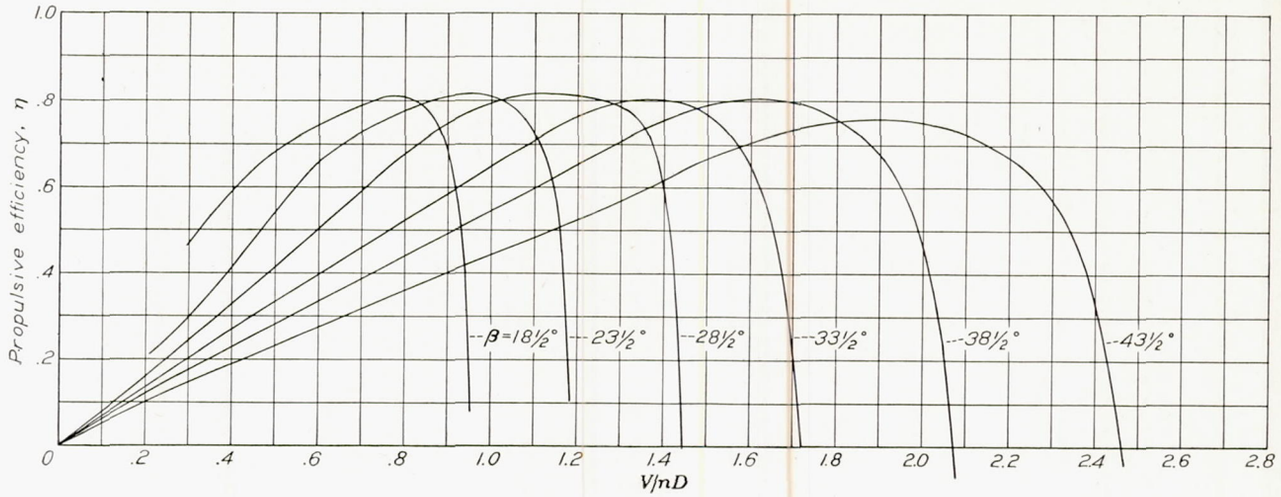

FIGURE 26.—Variation of propulsive efficiency with blade angle. The 10.4-inch nacelles; 0.25c propeller location; C_L, 0.25; air flowing through cowling.

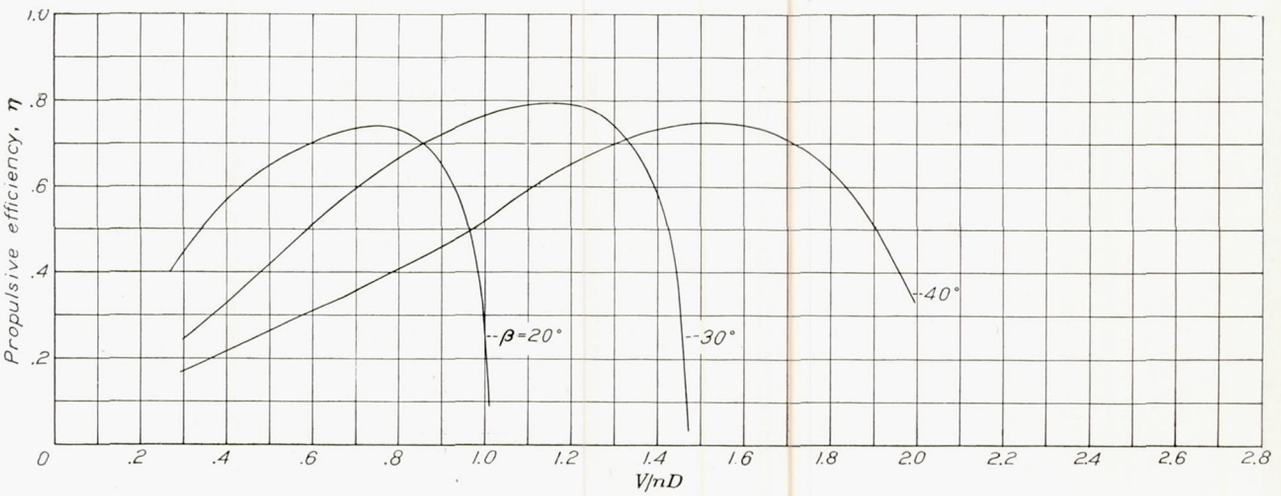

FIGURE 27.—Variation of propulsive efficiency with blade angle. The 7-inch nacelles; 0.40c propeller location; C_L, 0.25; cowling closed.

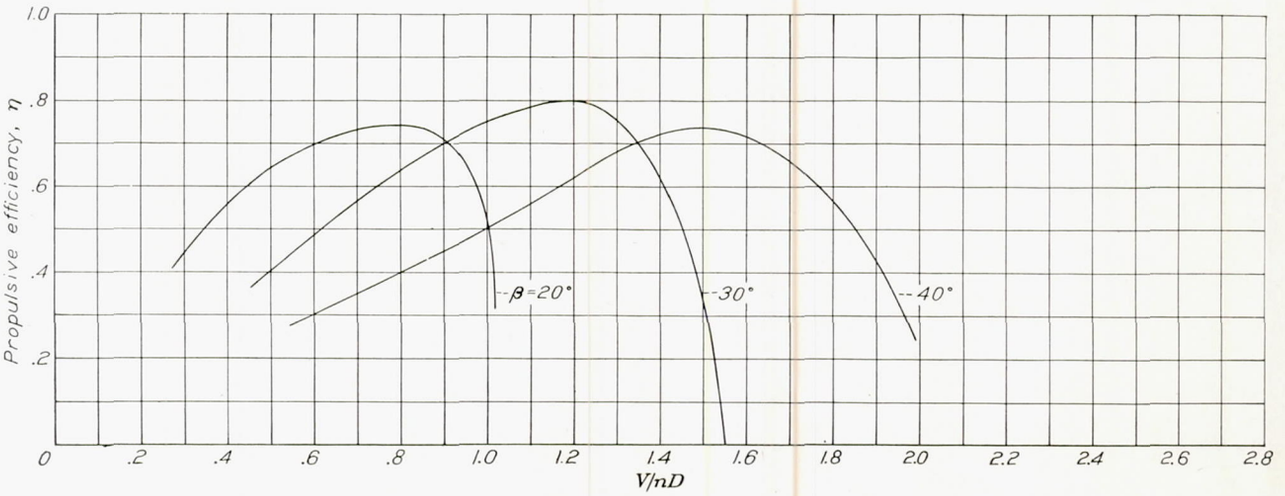

FIGURE 28.—Variation of propulsive efficiency with blade angle. The 7-inch nacelles; 0.25c propeller location; C_L, 0.25; cowling closed.

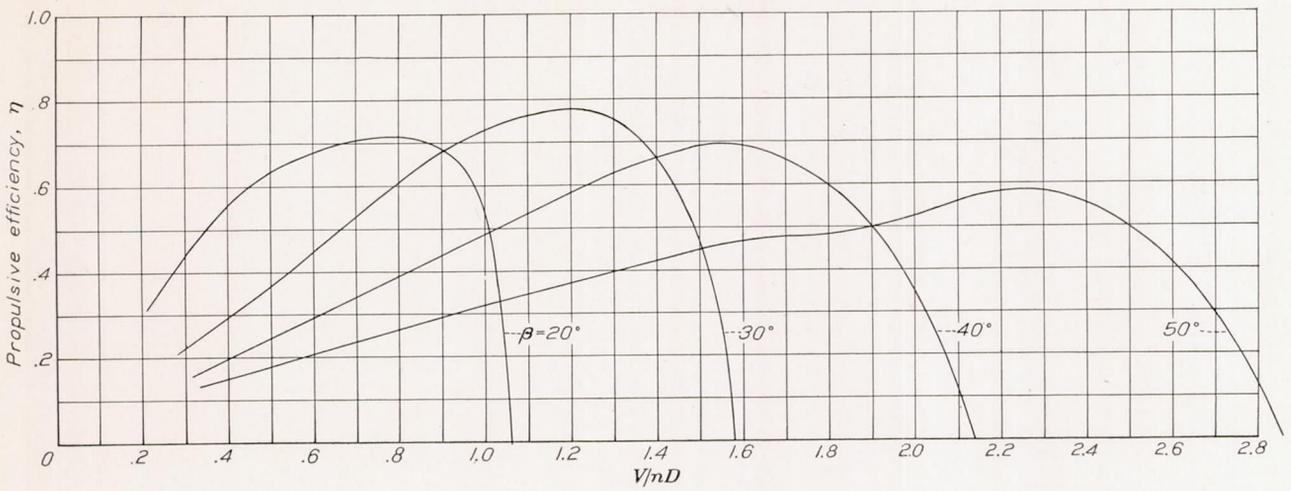

FIGURE 29.—Variation of propulsive efficiency with blade angle. The 7-inch nacelles; 0.13c propeller location; C_L, 0.25; cowling closed.

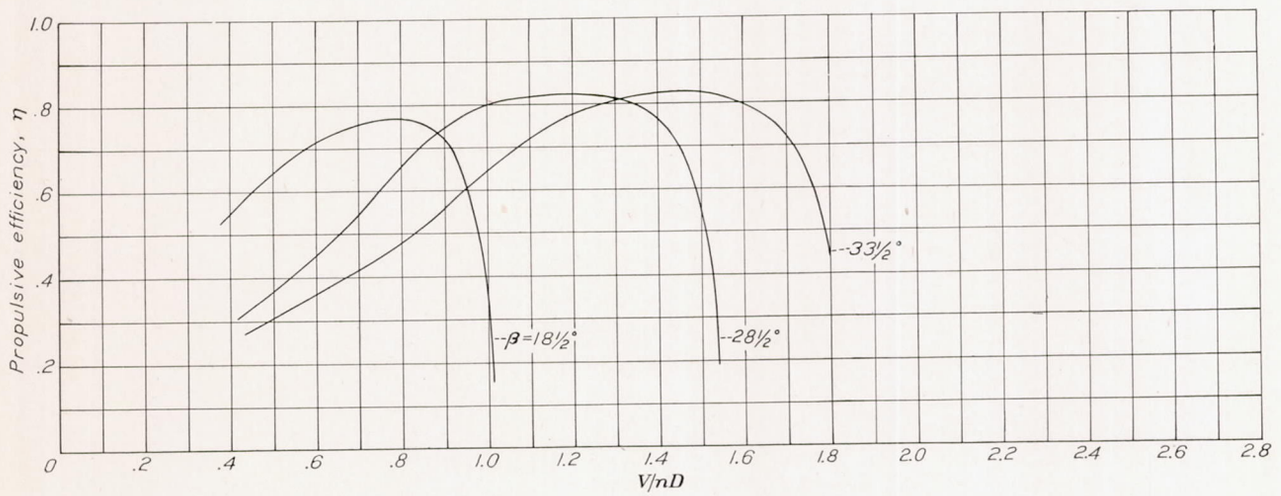

FIGURE 30.—Variation of propulsive efficiency with blade angle. The 20-inch nacelles; 0.40c propeller location; C_L, 0.25; cowling closed.

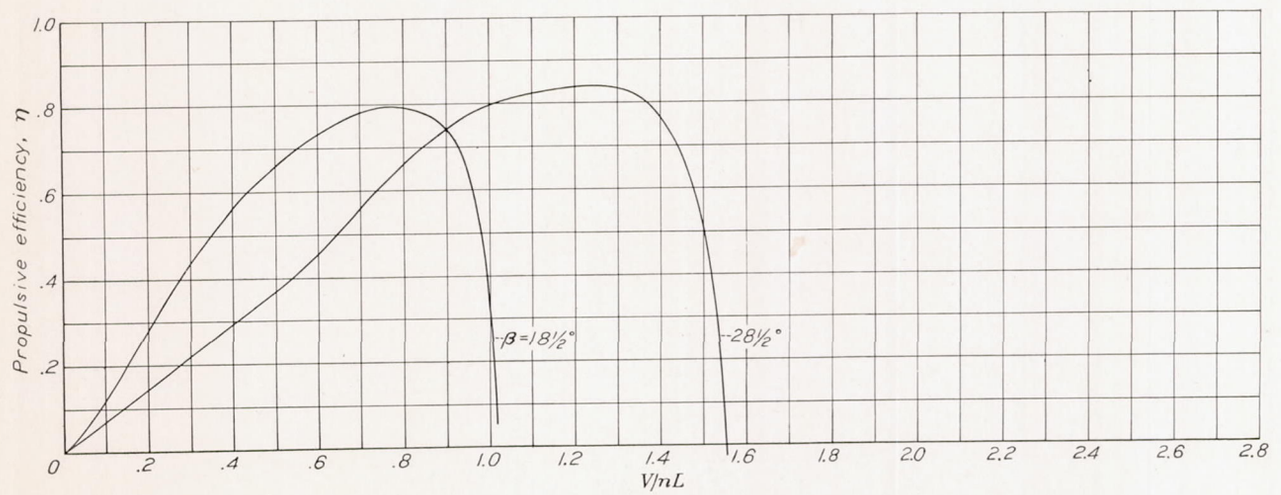

FIGURE 31.—Variation of propulsive efficiency with blade angle. The 20-inch nacelles; 0.25c propeller location; C_L, 0.25; cowling closed.

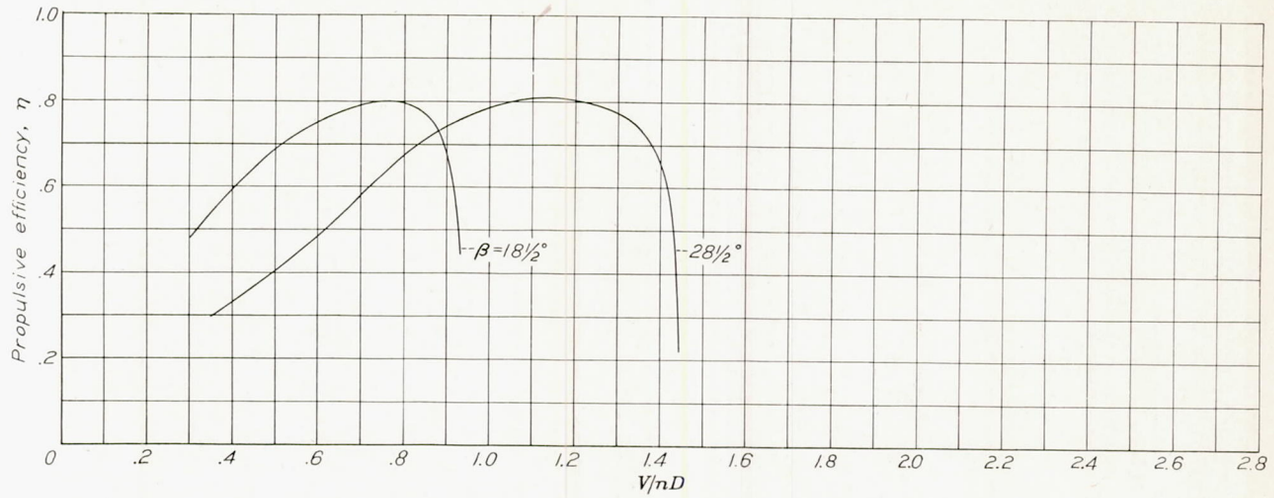

FIGURE 32.—Variation of propulsive efficiency with blade angle. The 10.4-inch nacelles; 0.40c propeller location; C_L, 0.25; cowling closed.

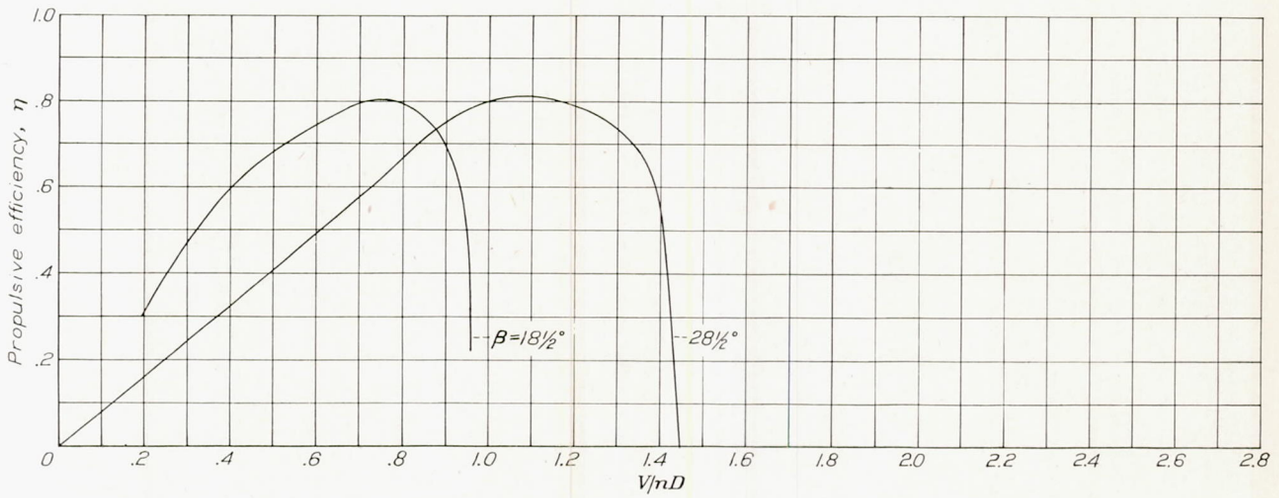

FIGURE 33.—Variation of propulsive efficiency with blade angle. The 10.4-inch nacelles; 0.25c propeller location; C_L, 0.25; cowling closed.

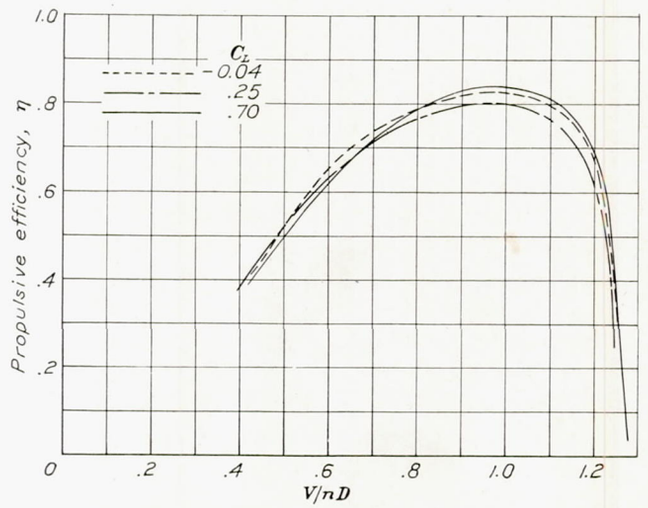

FIGURE 34.—Variation of propulsive efficiency with lift coefficient. The 20-inch nacelles; 0.40c propeller location; β, 23½°; air flowing through cowling.

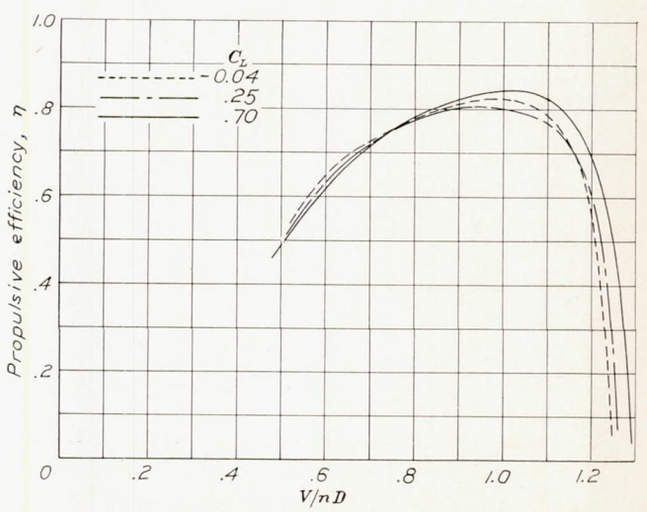

FIGURE 35.—Variation of propulsive efficiency with lift coefficient. The 20-inch nacelles; 0.25c propeller location; β, 23½°; air flowing through cowling.

OVER-ALL EFFICIENCY

As previously mentioned, neither the nacelle drag coefficient C_{D_F} nor the propulsive efficiency η alone is a sufficient measure of the efficiency of the conversion of engine power into the power available for propelling the airplane. A propulsion system should be credited only with the power available to pull the airplane minus the power plant through the air. Values of maximum over-all efficiency for propeller locations at 0.25c are plotted in figure 38 against nacelle size and an almost linear relation is shown. It is of importance to note that, for the nacelle with $D_N/t_w=1.5$, only about two-thirds of the engine power is usefully employed.

The variation in maximum over-all efficiency with lift coefficient is shown in figure 39 for the 10.4-inch and the 20-inch nacelles. The over-all efficiency is highest with the nacelle axis parallel to the relative wind ($C_L=-0.04$) and lowest at the high-speed lift coefficient. The efficiencies for the 0.25c and 0.40c propeller locations are similar, with a slightly higher efficiency indicated for the 0.25c location with the smaller nacelle. The comparison given in figure 39 is made for $\beta=23\frac{1}{2}°$, and is slightly unfair at $C_L=0.25$ to the 20-inch nacelle with propeller at 0.25c. This installation has a maximum efficiency at a somewhat higher blade angle than $23\frac{1}{2}°$ and, if the comparison had been made for this condition, the values for the 0.25c and 0.40c propeller locations would have been in essential agreement. On the basis of over-all efficiencies, it may be concluded that the 0.25c location is most favorable for the small nacelles and that, for the 20-inch nacelles, the 0.25c and 0.40c propeller locations are of equal merit.

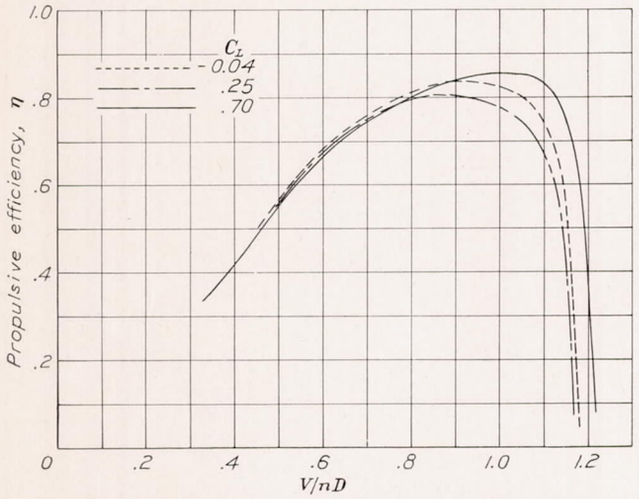

FIGURE 36.—Variation of propulsive efficiency with lift coefficient. The 10.4-inch nacelles; 0.40c propeller location; β, $23\frac{1}{2}°$; air flowing through cowling.

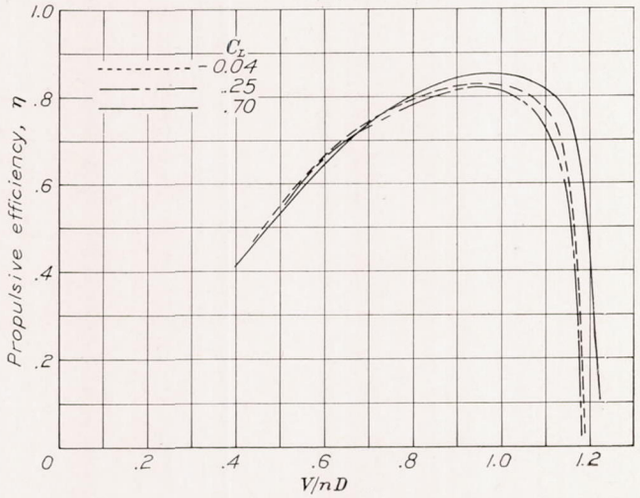

FIGURE 37.—Variation of propulsive efficiency with lift coefficient. The 10.4-inch nacelles; 0.25c propeller location; β, $23\frac{1}{2}°$; air flowing through cowling.

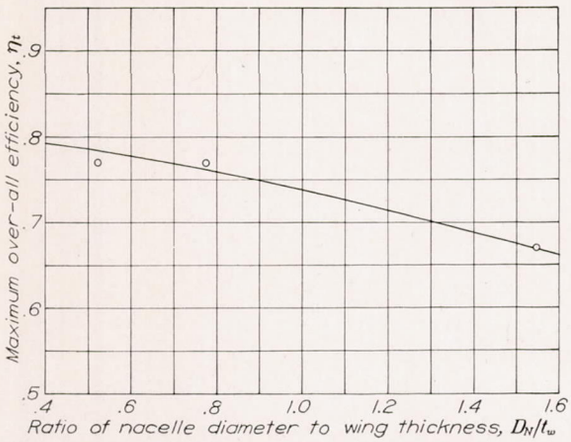

FIGURE 38.—Variation of maximum over-all efficiency with nacelle size. The 0.25c propeller location; C_L, 0.25; β, approximately 30°; air flowing through cowling.

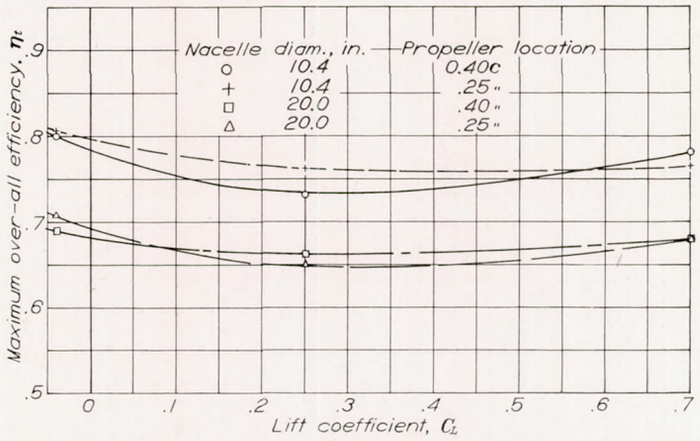

FIGURE 39.—Variation of maximum over-all efficiency with lift coefficient. Various nacelle arrangements; β, $23\frac{1}{2}°$; cowling closed.

POWER-ON CHARACTERISTICS

The effect of propeller operation on the aerodynamic characteristics of an airplane is primarily dependent on the amount of thrust delivered by the propellers and, for a given thrust, is relatively independent of moderate changes in blade angle, V/nD, propulsive efficiency, and propeller diameter. In order to describe the conditions of propeller operation, use is made of an index thrust coefficient that takes the form

$$T_{c_0}'=\frac{T_0}{qS}=\frac{P\eta_0}{qSV}$$

where η_0 is the propulsive efficiency at $C_L=0.25$ for the conditions of V/nD and blade angle at which the tests were made. The index thrust coefficient has the char-

acteristics and form of a drag coefficient and is essentially independent of the combination of V/nD and blade angle that produces the thrust; it is exactly equal to the amount of drag that the thrust would counterbalance at the standard or index condition and, at any other value of lift coefficient, differs from the true thrust coefficient only by the variation in propulsive efficiency between the two conditions.

The effect of propeller operation on the lift of the model is shown in figures 40 to 42 for three of the nacelle installations. Results are given for the flap neutral and the flap deflected 60°.

For the model with flaps neutral, the effect of the

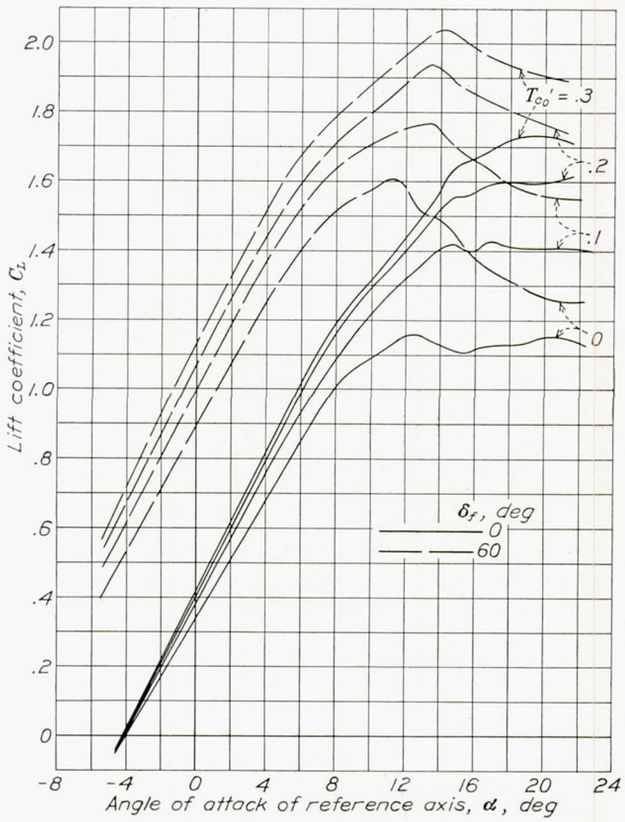

FIGURE 40.—Effect of propeller operation on lift coefficient of the model for various index thrust coefficients. The 20-inch nacelles; 0.40c propeller location.

propeller operation in each case is to increase slightly the slope of the lift curve and to increase greatly the maximum lift coefficient. With the flaps deflected, the slope of the lift curve and the maximum lift coefficient are not so greatly increased by the propeller operation. With increasing values of T_{c_0}', the maximum lift with flaps retracted approaches that for the flaps-deflected condition. The large increase in the maximum lift coefficient between the propeller-removed condition and the power-on condition with $T_{c_0}'=0.1$ (fig. 40) is due to the effect of the slipstream in decreasing the wing-nacelle interference. The maximum lift coefficients determined with freewheeling propellers were about the same as those for the propeller-off condition.

The large increase in maximum lift due to the propeller operation with the small propellers and nacelles

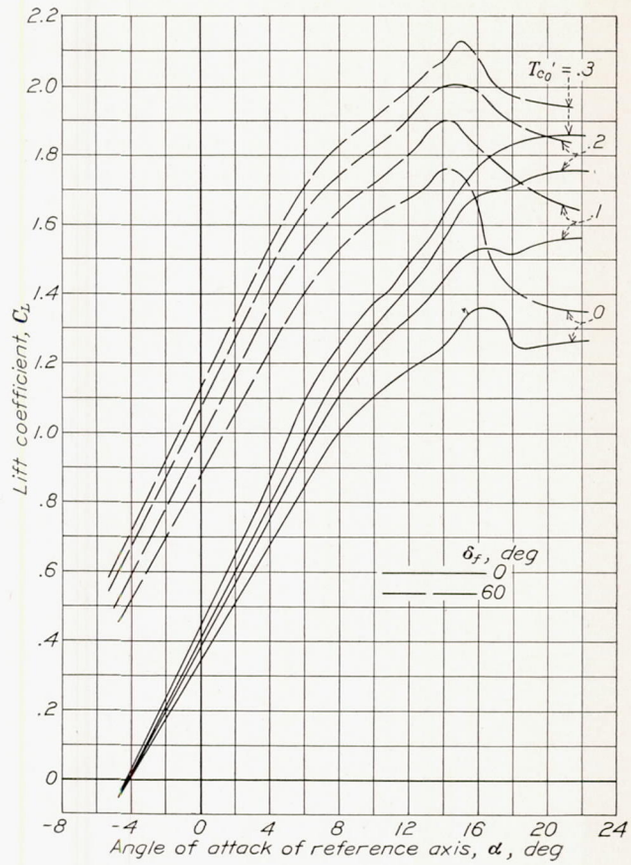

FIGURE 41.—Effect of propeller operation on lift coefficient of the model for various index thrust coefficients. The 10.4-inch nacelles; 0.25c propeller location.

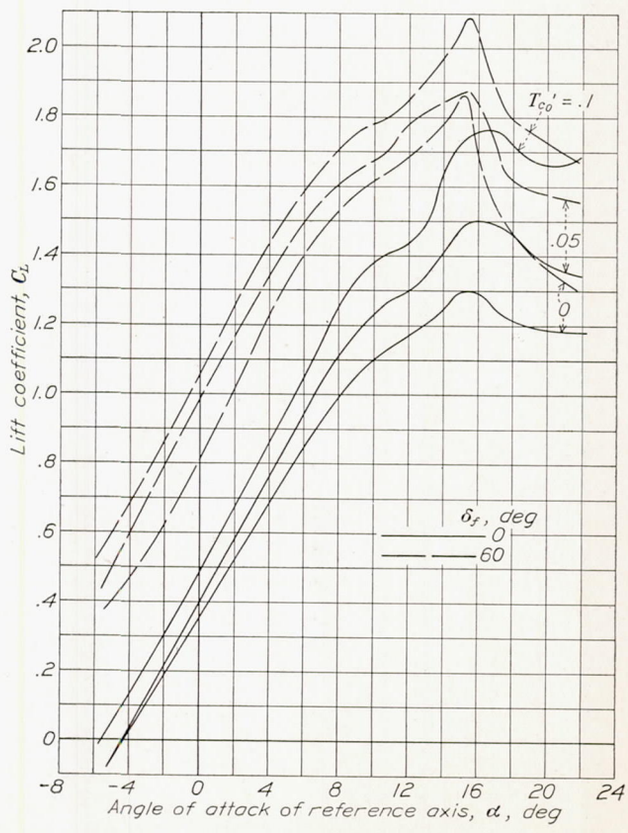

FIGURE 42.—Effect of propeller operation on lift coefficient of the model for various index thrust coefficients. The 7-inch nacelles; 0.13c propeller location.

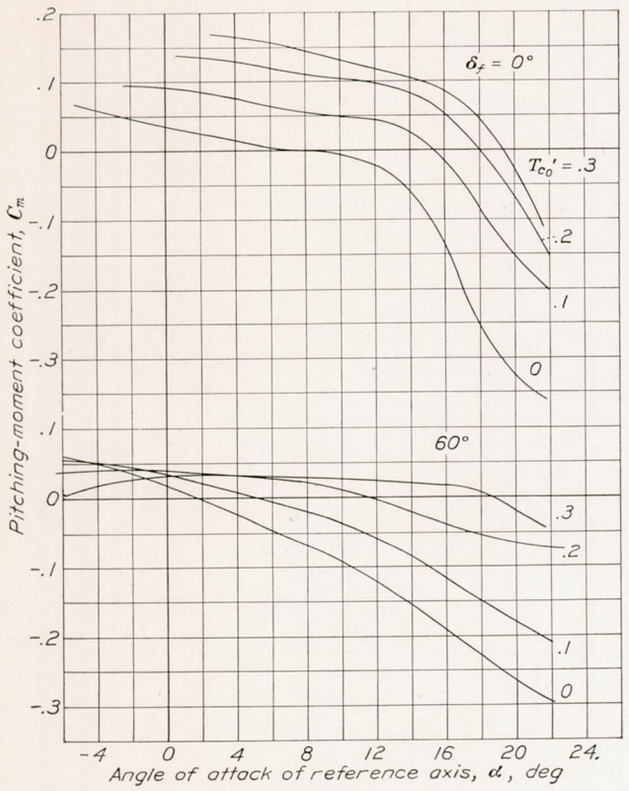

FIGURE 43.—Variation of pitching-moment coefficient of the model with index thrust coefficient. The 20-inch nacelles; 0.40c propeller location.

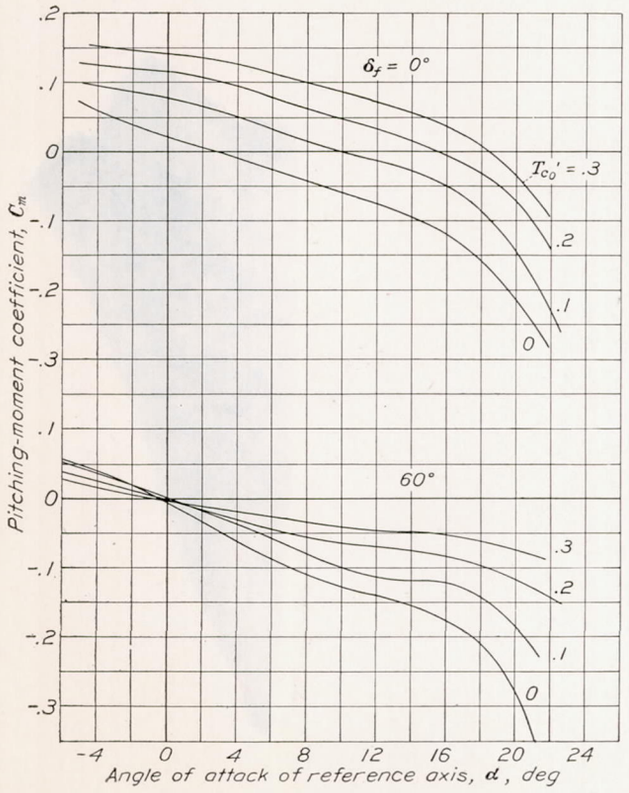

FIGURE 44.—Variation of pitching-moment coefficient of the model with index thrust coefficient. The 10.4-inch nacelles; 0.25c propeller location.

(fig. 42) is striking. The low test values of T_{c_0}' for this case are due to the lower power input required by the small-diameter propellers. It should be pointed out that the slipstream velocity for $T_{c_0}'=0.1$ with the 24-inch propellers is similar to that for $T_{c_0}'=0.3$ with the 39-inch propellers. The wing area immersed in the slipstream of the small propellers is only about 0.6 as much as for the large propellers and a corresponding decrease in slipstream effect would normally be expected.

The effects of the propeller operation on the pitching-moment coefficient, for the various thrust coefficients and nacelle installations, are shown in figures 43 to 45.

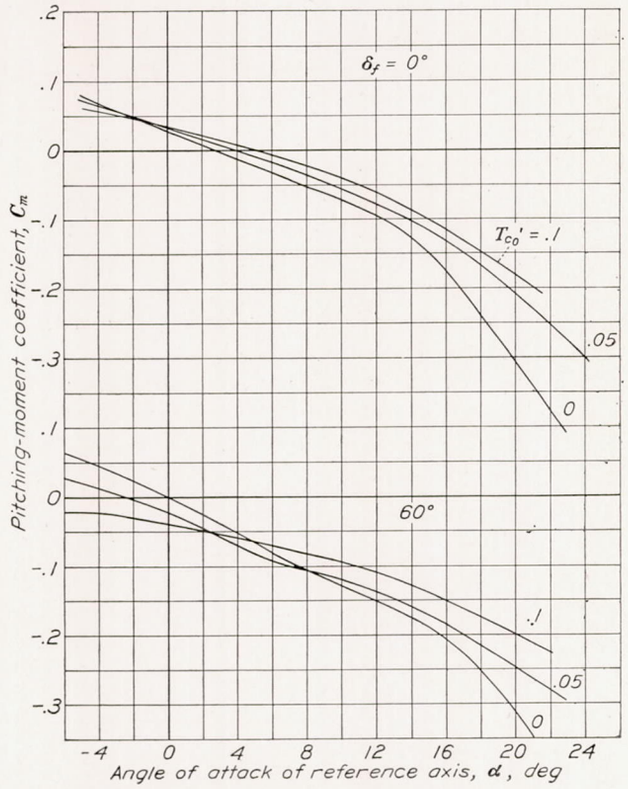

FIGURE 45.—Variation of pitching-moment coefficient of the model with index thrust coefficient. The 7-inch nacelles; 0.13c propeller location.

With the flap neutral, the principal effect of the propeller operation is to change the elevator angle required for balance. The pitching-moment curves are of similar shape and, except in the negative angle-of-attack range, the curves are similar to the ones that might be obtained by a shift of the tail angle. With the flaps deflected, the slope of the pitching-moment curve is greatly decreased with increasing thrust with the result that, for extreme conditions (fig. 43 at $T_{c_0}'=0.3$), instability is indicated over a considerable range of angles of attack. The pitching-moment curves for the 20-inch and the 10.4-inch nacelle installations, although similar in shape and in general characteristics, are somewhat different in numerical

value. The small nacelle installation, which was tested with the 24-inch-diameter propellers, shows smaller effects of the power on the pitching moment although, in general, the effects are similar to those for the large nacelle.

CONCLUSIONS

1. The over-all efficiency of propulsion of the four-engine model at conditions of high-speed flight decreased linearly from about 77 to 67 percent as the nacelle diameter was increased from 0.5 to 1.5 times the wing thickness.

2. Nacelle installations with the propeller located $0.25c$ ahead of the leading edge were more efficient than those having the propeller at the $0.40c$ location in the range of ratios of nacelle diameter to wing thickness from about 0.5 to 1. For a value of the ratio of nacelle diameter to wing thickness of 1.5, the $0.25c$ and the $0.40c$ propeller locations were of about equal merit. The propulsive efficiencies for small nacelle-propeller installations close to the leading edge of a wing were lower than for the $0.25c$ location.

3. The propulsive efficiency of the 39-inch-diameter propeller was about the same for tests made with the 10.4-inch and the 20-inch nacelles.

4. The values of propulsive efficiency determined with or without air flowing through the cowling were in substantial agreement.

5. The maximum lift-drag ratio of the model was substantially reduced by nacelles of even very small ratios of nacelle diameter to wing thickness.

6. The nacelle installations contributed destabilizing moments to the airplane that must be considered in the tail design.

7. The maximum lift coefficient of the airplane with propeller removed was decreased about 9 percent for the nacelle installation having a value of the ratio of nacelle diameter to wing thickness of 1.50 and was slightly increased by small nacelles.

LANGLEY MEMORIAL AERONAUTICAL LABORATORY,
NATIONAL ADVISORY COMMITTEE FOR AERONAUTICS,
LANGLEY FIELD, VA., *May 17, 1939.*

REFERENCES

1. DeFrance, Smith J.: The N. A. C. A. Full-Scale Wind Tunnel. Rep. No. 459, NACA, 1933.
2. Robinson, Russell G., and Becker, John V.: High-Speed Tests of Radial-Engine Cowlings. Rep. No. 745, NACA, 1942.
3. Theodorsen, Theodore, Brevoort, M. J., and Stickle, George W.: Full-Scale Tests of N. A. C. A. Cowlings. Rep. No. 592, NACA, 1937.

U. S. GOVERNMENT PRINTING OFFICE: 1942

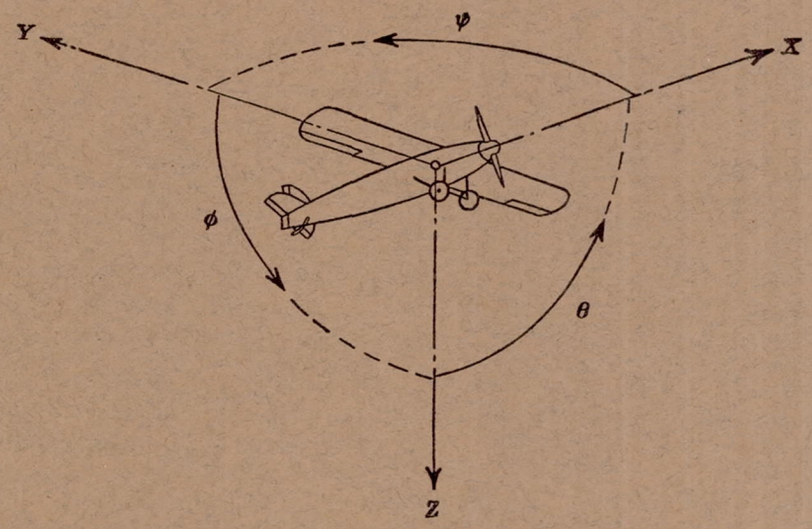

Positive directions of axes and angles (forces and moments) are shown by arrows

Axis		Force (parallel to axis) symbol	Moment about axis			Angle		Velocities	
Designation	Symbol		Designation	Symbol	Positive direction	Designation	Symbol	Linear (component along axis)	Angular
Longitudinal	X	X	Rolling	L	$Y \longrightarrow Z$	Roll	φ	u	p
Lateral	Y	Y	Pitching	M	$Z \longrightarrow X$	Pitch	θ	v	q
Normal	Z	Z	Yawing	N	$X \longrightarrow Y$	Yaw	ψ	w	r

Absolute coefficients of moment

$C_l = \frac{L}{qbS}$ (rolling) $\quad C_m = \frac{M}{qcS}$ (pitching) $\quad C_n = \frac{N}{qbS}$ (yawing)

Angle of set of control surface (relative to neutral position), δ. (Indicate surface by proper subscript.)

4. PROPELLER SYMBOLS

D Diameter

p Geometric pitch

p/D Pitch ratio

V' Inflow velocity

V_s Slipstream velocity

T Thrust, absolute coefficient $C_T = \frac{T}{\rho n^2 D^4}$

Q Torque, absolute coefficient $C_Q = \frac{Q}{\rho n^2 D^5}$

P Power, absolute coefficient $C_P = \frac{P}{\rho n^3 D^5}$

C_s Speed-power coefficient $= \sqrt[5]{\frac{\rho V^5}{P n^2}}$

η Efficiency

n Revolutions per second, rps

Φ Effective helix angle $= \tan^{-1}\left(\frac{V}{2\pi r n}\right)$

5. NUMERICAL RELATIONS

1 hp=76.04 kg-m/s=550 ft-lb/sec

1 metric horsepower=0.9863 hp

1 mph=0.4470 mps

1 mps=2.2369 mph

1 lb=0.4536 kg

1 kg=2.2046 lb

1 mi=1,609.35 m=5,280 ft

1 m=3.2808 ft